Advanced Materials

Recent Advances in Two Dimensional Inorganic Nanomaterials for SERS sensing

--Manuscript Draft--

Manuscript Number:	adma.201803432R2
Full Title:	Recent Advances in Two Dimensional Inorganic Nanomaterials for SERS sensing
Article Type:	Review
Section/Category:	By Invitation Only: Sungkyunkwan University Special Issue
Keywords:	Raman enhancement; 2D material; Chemical sensors; nanomaterials; metal chalcogenides,
Corresponding Author:	Chan-Hwa Chung Sungkyunkwan University Suwon, KOREA, REPUBLIC OF
Additional Information:	
Question	**Response**
Please submit a plain text version of your cover letter here.	Dear Dr. Duoduo Liang I am herewith submitting our revised manuscript entitled “Recent Advances in Two Dimensional Inorganic Nanomaterials for SERS sensing” for your consideration to publish in the journal “Advanced Materials”. We have carried out the required revision in accordance with the suggestions of the two Reviewers and have given the response to all their comments. We have also highlighted (blue colour) the necessary changes that were made on the revised manuscript. I request that the revised manuscript may please be considered further for publication in the journal
Do you or any of your co-authors have a conflict of interest to declare?	No. The authors declare no conflict of interest.
Corresponding Author Secondary Information:	
Corresponding Author's Institution:	Sungkyunkwan University
Corresponding Author's Secondary Institution:	
First Author:	Karthick Kannan Padmanathan
First Author Secondary Information:	
Order of Authors:	Karthick Kannan Padmanathan
	Prabakaran Shankar
	Chris Blackman
	Chan-Hwa Chung
Order of Authors Secondary Information:	
Abstract:	Surface enhanced Raman scattering (SERS) is a powerful and sensitive analytical tool that has found application in chemical and biomolecule analysis and environmental monitoring. Since its discovery in the early 70's, a variety of materials ranging from noble metals to nanostructured materials have been employed as SERS substrates. In recent years, two dimensional inorganic materials have found wide interest in the development of SERS-based chemical sensors owing to their unique thickness dependent physico-chemical properties with enhanced chemical-based charge-transfer processes. Here, recent advances in the application of various two dimensional inorganic nanomaterials, including graphene, boron nitride, semiconducting metal oxides and transition metal chalcogenides, in chemical detection via SERS are

	presented. The background of the SERS concept, including its basic theory and sensing mechanism, along with the salient features of different nanomaterials used as substrates in SERS, extending from monometallic nanoparticles to nano-metal oxides, are comprehensively discussed. The importance of two dimensional inorganic nanomaterials in SERS enhancement, along with their application towards chemical detection, is explained in detail with suitable examples and illustrations. In conclusion, some guidelines are presented for the development of this promising field in the future.

Recent Advances in Two Dimensional Inorganic Nanomaterials for SERS sensing

Padmanathan Karthick Kannan[1+], Prabakaran Shankar[2,3+], Chris Blackman[4] and Chan-Hwa Chung[1*],

[1]School of Chemical Engineering, Sungkyunkwan University, Suwon 16419, Republic of Korea

[2]School of Advanced Materials Science and Engineering, Sungkyunkwan University, Suwon 16419, Republic of Korea

[3]Institute of Innovative Science and Technology, Tokai University, Hiratsuka, Kanagawa 259 1292, Japan

[4]Department of Chemistry, University College London, London, WC1H 0AJ, United Kingdom

*E-mail: chchung@skku.edu

[+] These authors contributed equally

Contents

ABSTRACT

Surface enhanced Raman scattering (SERS) is a powerful and sensitive analytical tool that has found application in chemical and biomolecule analysis and environmental monitoring. Since its discovery in the early 70's, a variety of materials ranging from noble metals to nanostructured materials have been employed as SERS substrates. In recent years, two dimensional inorganic materials have found wide interest in the development of SERS-based chemical sensors owing to their unique thickness dependent physico-chemical properties with enhanced chemical-based charge-transfer processes. Here, recent advances in the application of various two dimensional inorganic nanomaterials, including graphene, boron nitride, semiconducting metal oxides and transition metal chalcogenides, in chemical detection *via* SERS are presented. The background of the SERS concept, including its basic theory and sensing mechanism, along with the salient features of different nanomaterials used as substrates in SERS, extending from monometallic nanoparticles to nano-metal oxides, are comprehensively discussed. The importance of two dimensional inorganic nanomaterials in SERS enhancement, along with their application towards chemical detection, is explained in detail with suitable examples and illustrations. In conclusion, some guidelines are presented for the development of this promising field in the future.

1 Introduction

Over the past three decades research and development on fabrication of chemical sensors and biosensors for the detection of toxic chemicals, industrial waste, environmental pollutants, chemical warfare agents and biological indicators has been an active area in analytical sciences[1]. A variety of techniques have been used as a transducing method in chemical sensing including gas chromatography with mass spectroscopy[2], optical[3], electrochemical[4], conductometric[5] and gravimetric[6]. Despite the large volume of research on chemical sensing, the process of developing a chemical sensor with high sensitivity and selectivity is still highly challenging and real time applications, such as environmental monitoring, explosive detection and medical diagnosis, where rapid detection at trace levels is required, can be a particular issue. Among various sensing modalities, optical methods have the potential to sense chemicals at very short detection times with high selectivity and over a wide concentration range[7]. In addition, optical methods can be operated in a 'stand-off' mode where the analyte and the sensing material are separated from each other during measurement. A variety of optical spectroscopy techniques, including UV-visible[8], photoluminescence[9], fluorescence[10], reflectance[11] and infra-red (IR)[12] have been employed in chemical sensing. Surface enhanced Raman spectroscopy (SERS), which has been demonstrated to detect down to the single molecule level with high specificity, has also attracted much attention. SERS not only provides high sensitivity and the ability to provide a specific 'fingerprint', but is also non-destructive, can be operated in real time operation and allows *in-situ* remote sensing[13]. Numerous review articles have discussed recent developments in the use of SERS for various biomedical applications, e.g. biomolecule investigation[14,15], blood analysis[16] and cancer cell detection[17] amongst others. In terms of

materials requirements, numerous review articles are available in which the fabrication of SERS active substrates are based on nanomaterials such as metal nanoparticles[18], metal oxide nanostructures[19], carbon nanotube and graphene[20,21], have been discussed. In recent times, two dimensional inorganic nanomaterials have been attracting wide interest for use in SERS sensing because of their interesting layer dependent optical properties[22] and their very large surface to volume ratio (**Figure 1**)[23]. This review article will focus on the application of various two dimensional inorganic nanomaterials in SERS sensing, including a description of the SERS sensing mechanism and a demonstration of the importance of two dimensional inorganic nanomaterials for SERS sensing by highlighting some recent advances on the use of various 2D-nanomaterials.

2 SERS- Background

Raman spectroscopy has been used an analytical tool since its discovery in 1928 by Raman and Krishnan[24]. Like other spectroscopic techniques such as Fourier transform infra-red, UV-visible and fluorescence spectroscopy, the data obtained from Raman spectroscopy can be used as a compound fingerprint[25], and it is able to deliver information on chemicals and biomolecules at the molecular level without the requirement for a labelling process, thus demonstrating potential for sensing a wide range of analyte molecules[26]. Consequently Raman spectroscopy has been widely employed, particularly in biological and pharmaceutical applications[27] where it has been used for quantifying the active substances in different pharmaceutical formulations[28], for identifying cancer cells[29], for investigating the structures of various biomolecules[30], and for disease diagnosis and detection of pathologies[31–33]. However, Raman spectroscopy typically has

a very weak signal compared to that of fluorescence, with the magnitude of the Raman scattering cross-section being 14 orders of magnitude smaller than that of a fluorescence signal[34].

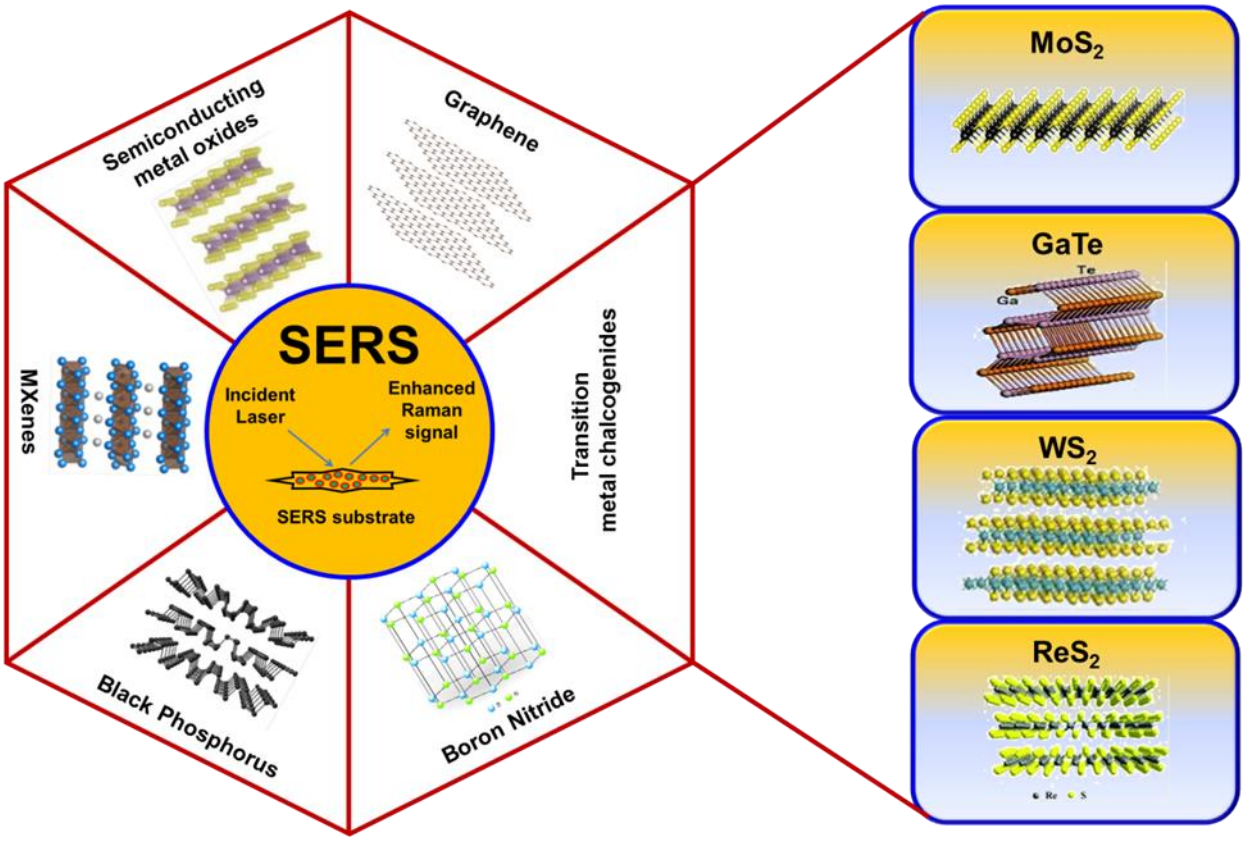

Figure 1. Various 2D nanomaterials employed in SERS sensing application.

Due to this drawback, the application of Raman spectroscopy in trace analysis has been limited, and in order to mitigate this problem it is essential to increase the cross-section of the Raman scattering in order to enhance the Raman signal.

In 1974 a research group comprising of Fleishmann, Hendra and McQuilian investigated the surface Raman spectrum of pyridine molecule adsorbed on an electrochemically roughened silver surface[35]. Later, in 1977, Jeanmaire and Van Duyne found that when a Raman scattering species is placed on or near a roughened noble metal surface the magnitude of the Raman signal was a million times more intense than that of a conventional Raman signal[36]. This phenomenon was later called Surface Enhanced Raman Scattering (SERS) and overcomes the issues associated with lack of sensitivity in conventional Raman Scattering[37]. Since the discovery of SERS there have been many research papers, review articles and book chapters that have appeared in the literature[26,38–44].

3 SERS- Basic Theory

The working principle of normal Raman spectroscopy is based on the occurrence of inelastic collision caused by molecules during their interaction with an electromagnetic field (EMF)[45]. In this process the photons generating the EMF can gain or lose energy from the molecules, resulting in a change in the frequency (or energy) of the scattered photons. The change in the energy value of the scattered photons with respect to the incident light gives the vibrational energy difference value, which is called Raman shift. Generally, the Raman shift is expressed in wavenumbers (cm^{-1}) and the respective data is called a Raman spectrum.

When an EMF from an incident photon interacts with a molecule, the photon is scattered and a dipole moment (μ_{ind}) is induced which is directly proportional to the polarizability (α_m) of the molecule. The relation between the incident EMF ($E_{incident}$) and the induced dipole moment (μ_{ind}) can be represented as[45,46]

$$\mu_{ind} = E_{incident} \bullet \alpha_m \quad (1)$$

The efficiency of the scattering process can be investigated by differential Raman scattering cross section and is defined as[43]

$$\text{Efficiency} = d\sigma_r/d\Omega \quad (2)$$

where, σ_r is the part of the cross section and $d\Omega$ is the element of the solid angle. For a given molecule the differential Raman cross section depends on the particular vibrational mode, and for a given medium the Raman cross section depends on the excitation wavelength of the incident light and the refractive index of the medium. In a typical Raman scattering event it has been shown that the cross-section per molecule is typically in the range of 10^{-31} to 10^{-29} cm^2 sr^{-1} (sr=steradian), which is significantly lower than the equivalent value obtained for fluorescence spectroscopy (10^{-16} cm^2 sr^{-1})[47], and consequently for most molecules Raman scattering is intrinsically weak. As a result it has been estimated that in Raman spectroscopy, for each approximately 10^6 – 10^9 photons incident on the sample only 1 photon undergoes an inelastic scattering event, and consequently the strength of the signal is very low. However in SERS, it is found that the Raman signal is enhanced when an EMF irradiation takes place near a nanostructured metallic surface such as such as Ag, Au or Cu. During irradiation of the metallic nanostructures at particular wavelengths, highly concentrated 'hot spots' are generated by

surface plasmon resonance[48,49]. These hot spots act as a signal amplification element and greatly enhance the Raman signal, with the calculated differential Raman cross-section value for a SERS experiment found to be very close to the cross section in fluorescence, and consequently a SERS measurement is possible even at the single molecule level. Many papers have been published attempting to explain the SERS enhancement mechanism [50–54], however it is generally accepted that two mechanisms are predominantly responsible for the Raman signal enhancement, an electromagnetic mechanism and a chemical mechanism. The electromagnetic contribution is related to the resonant excitation of the surface plasmons present on the metal surface whilst the chemical enhancement depends on the polarizability of the analyte molecule adsorbed on the metal surface.

As shown in Eqn.1 the physical parameter that characterizes the Raman scattering event is the induced dipole moment, and the two primary components of that scattering process are the local electric field (E_{loc}) and the molecular polarizability (α). Hence it can be understood why the two major enhancement mechanisms, *viz*. electromagnetic (EM) and chemical, are responsible for the enhancement of Raman signal in a SERS measuremement.

3.1 EM Enhancement

In this mechanism, the incident EM field and the scattered Raman field are amplified when the nanostructured metallic surface is illuminated with light that is in resonance with the frequency of localized surface plasmons present on the metallic surface (i.e. is at the same wavelength). The physics underlying this EM enhancement can be understood by considering a metallic nanosphere in an applied electric field. When an EM field (e.g. laser illumination) is incident on a metal nanoparticle, the oscillating electric field (amplitude E_0 and angular frequency ω_{inc})

present in the irradiation excites the electrons in the metal leading to a polarization of charge. This phenomenon is named as dipolar localized surface plasmon resonance. As a result of this polarization an induced dipole moment (μ_{ind}) is generated which is determined by the polarizability of the metal (α_{met}) and the amplitude of the incident electric field ($E_0(\omega_{inc})$), and can be represented as[55]

$$\mu_{ind} = \alpha_{met} E_0(\omega_{inc}) \quad (3)$$

In a typical Raman scattering event, the incident light induces a dipole moment on the molecule which is then scattered and recorded as the Raman signal. Thus Raman scattering involves a twofold process, comprising both excitation and the scattering of the incident light. Similarly, SERS is also a twofold process. However, the main difference is that in SERS there is an enhancement in the local EM field due to the presence of the hotspot on the metal nanoparticle, i.e. the inelastic scattering of the incident electric field $E_0(\omega_{inc})$ on the metal nanoparticle creates an enhanced local electric field $E_{loc}(\omega_{inc})$ in the vicinity of the metallic surface. The interaction of this local electric field on a molecule adsorbed on the metallic surface generates a dipole moment which can be expressed as[55]

$$\mu_{ind} = \alpha_{mol} E_{loc}(\omega_{inc}) \quad (4)$$

where, α_{mol} is the polarizability of the molecule and $E_{loc}(\omega_{inc})$ is the enhanced local electric field. In the classical theory of Raman scattering, the existence of inelastic scattering for a vibrating molecule can be explained using two parameters *viz*. the incident local electric field $E_{loc}(\omega_{inc})$ and the angular eigen frequency (ω_{vib}) of the vibrating molecule. As a result of this inelastic scattering, three dipole components occur : $\mu_{ind}(\omega_{inc})$, $\mu_{ind}(\omega_{inc} - \omega_{vib})$ and $\mu_{ind}(\omega_{inc}+\omega_{vib})$,

which correspond to three scattering components, named Rayleigh, Stokes and anti-Stokes respectively.

The enhancement of the scattered Stokes (or anti-Stokes) field is dependent on the resonance frequency of the surface plasmons present on the surface of the metal sphere; considering the intensity of the incident EM field and the Stokes scattering field, the overall SERS enhancement intensity can be given as

$$I_{SERS} = I_{inc}(\omega_{inc})\, I(\omega_s) \quad (5)$$

where $\omega_s = \omega_{inc} - \omega_{vib}$

Eq. 5 can be rewritten in terms of the electric field E_{inc} and E_{loc} which is given as[55]

$$I_{SERS} = |E_{inc}(\omega_{inc})|^2\, |E(\omega_s)\,|^2 \quad (6)$$

where $E_{inc}(\omega_{inc})$ is the local electric field enhancement factor with frequency ω_{inc} and $E(\omega_s)$ is the electric field enhancement factor at the Stokes shifted frequency ω_s. If both these electric field values are close to each other, then the SERS intensity enhancement becomes

$$I_{SERS} = |E(\omega_{inc})|^4 \quad (7)$$

From this relation, it can be understood that the SERS enhancement from the EM mechanism is equal to the fourth power of the electric field enhancement value ($E(\omega_{inc})$) at the Stokes shifted frequency ω_s.

3.2 Chemical Enhancement

The second major mechanism of SERS enhancement is the chemical effect, where the essential prerequisite is direct contact between the SERS-active metal and the analyte molecule. Chemical enhancement is often termed as a ‘first layer’ effect, in which the major phenomenon is the formation of an adsorbate-surface complex as a result of electronic coupling between the

molecule and the metal. This interaction, in which electrons from the Fermi level of the metal transfer to the lowest unoccupied molecular orbital of the molecule, results in the formation of charge transfer intermediates with higher Raman cross-section than that of the free molecule. When the frequency of the incident photon ω_{inc} is in resonance with the charge transfer transition of the newly formed complex the scattered Stokes intensity contains information about the vibrational state of the molecule. In general, the magnitude of the chemical enhancement effect is of 10^0-10^2 and much weaker than the EM enhancement.

4 Nanomaterials for Sensing

The primary requirement for the SERS signal enhancement is the presence of highly populated hot spots on a metallic surface and hence much research has been focused on developing materials and substrates with a high density of hot-spots. Many materials have been investigated for the detection of various analyte probes including noble metal nanoparticles, composite nanoparticles, core-shell nanoparticles, metal oxides, single element semiconductors, and some nano-metal based hybrid materials[56–59]. Factors such as the size, orientation, shape, inter-particle distance, dielectric properties and surface characteristics of the materials strongly influence the magnitude of the enhancement observed, and several reviews are available in which the use of different materials in SERS sensing have been reviewed in detail[60–62].

Metals such as gold (Au), silver (Ag) and copper (Cu) have traditionally been used as the substrate materials in SERS sensors[63–65], with Au and Ag having high air stability whilst Cu is, as expected, more reactive[49]. Various nanostructured materials are being developed and

investigated in SERS chemical sensing applications[66] with a plethora of nanostructures being investigated, such as one dimensional (1D) nanostructures including nanorods[67] and nanowires[68], two dimensional (2D) nanostructures including nanoplates[69], nanosheets[70], nanoprisms[71], and nanodisks[103] and three dimensional nanostructures (3D) including nanostars[104], nanocages[74], nanoflowers[75], nanodendrites[76]. **Figure 2** shows scanning electron micrographs of various morphologies of gold and silver nanostructures employed for SERS sensing.

In general, preparation of SERS substrates can be categorized under three different methodologies: 1) synthesis of SERS active metallic nanoparticles in suspension 2) immobilization of metallic nanostructures on solid substrates and 3) direct fabrication of metallic nanostructures on a suitable substrate using thin film deposition and lithorgraphy processes. In the following section, the application of different materials and substrates on the development of SERS based chemical sensors are briefly reviewed and highlighted, however the use of metallic nanoparticles in suspension has some limitations as the method is not feasible for the development of solid state SERS chemical sensors[62].

4.1 Metallic Au, Ag and Cu nanoparticles

During the early stage in SERS exploration, colloidal suspensions of noble metals such as Au and Ag were used as the active SERS substrates. Ag nanoparticles are shown to exhibit a large enhancement in SERS intensity, greater than that of Au nanoparticles, however under physiological conditions Ag nanoparticles are unstable, in contrast to Au nanoparticles[61]. Colloidal metal suspensions are very well suited for solution phase SERS study and simple

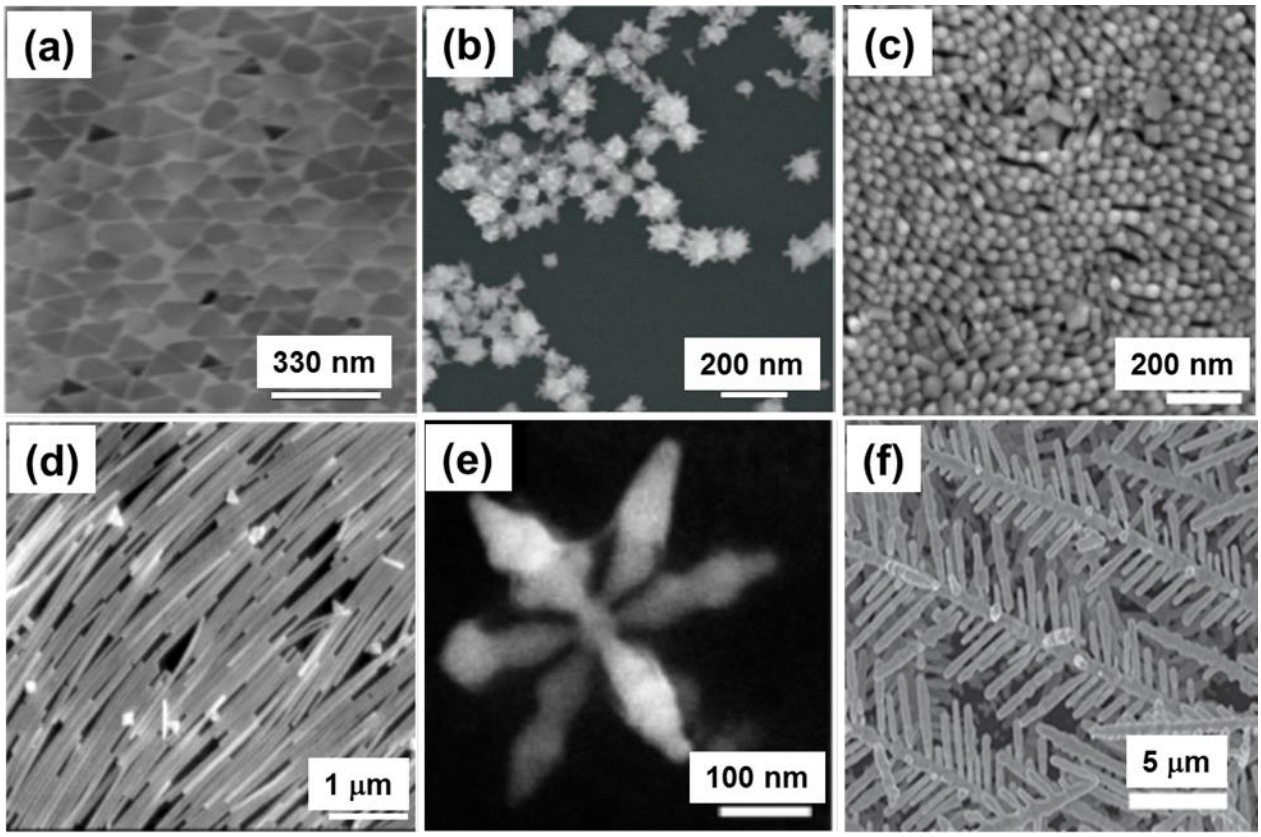

Figure 2. SEM images of various Au and Ag based nanostructures employed in the fabrication of SERS substrates. (a) Au nanoprism (b) Ag nanoflower (c) Au nanorod (d) Ag nanowire (e) Ag nanostar (f) Ag nanodendrite [71,75,77–80]

chemical methods can be used for their preparation, however the major limitation encountered in their use is the broadening of the resonance level due to non-uniformity in the distributions of particle size and shape. In addition colloid solutions have a tendency to coagulate and as a result show high instability in SERS measurements. For sensing using solid-state materials, thin films of metal islands have been used as the substrate material, however this approach was found to be unreliable due to the perturbation of the metastable nanostructures comprising the metal island substrates. Compared to colloids and metal island thin films, nanoparticles of noble metals exhibit very large SERS enhancement and there are many reports available on the use of monometallic nanoparticles in SERS sensing applications[18,81,82]. The size and shape of the monometallic nanoparticles plays an important role and it has a strong influence on the SERS enhancement, for instance it has been inferred using three-dimensional finite difference time-domain numerical simulation thatAu nanoparticles with vertical variations of surface have larger field enhancements than that of structures with horizontal variations in SERS detection of Rhodamine 6G[83]. The shape of the Au nanoparticles has also been found to be critical[84], with a greater enhancement in the SERS signal (**Figure 3e**) for nanostars (**Figure 3d**) compared to nanosphere aggregates (**Figure 3b),** nanotriangles (**Figure 3c**) and nanospheres (**Figure 3a**), which was attributed to the number of hotspots expected in each shape, being greatest in the case of nanostars due to a relative increase in edge area. The influence of gold and silver particle shapes and sizes in SERS enhancement has been investigated theoretically using T-matrix calculations[85] where it was found that the degree of SERS enhancement is determined only by the shape and not the size or material. There are relatively few papers available on the systematic investigation of the effect of particle size and shape on the SERS enhancement of colloidal silver nanoparticles[58,83–86].

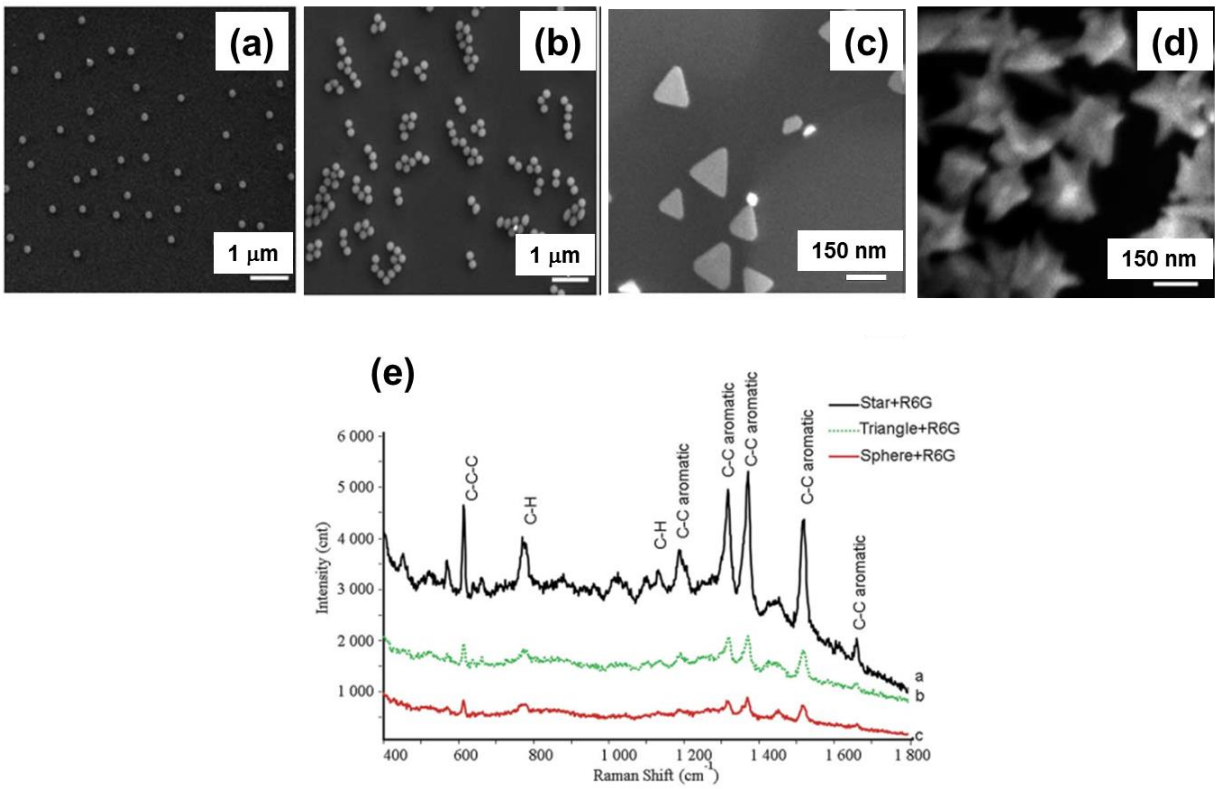

Figure 3. SEM images of (a) Au nanospheres (b) Au aggregated nanospheres (c) Au nanotriangles (d) Au nanostars. (e) Comparative SERS spectra measured for Au nanostar, Au nanotriangle and Au aggregated nanosphere samples in 1 M R6G solution [84]**;** Excitation wavelength – 785 nm; Concentration of Ag nanosamples – 3×10^9 particles per mL. Substrate – CaF_2;

4.2 Bimetallic Alloy/Core-Shell Nanoparticles

Like monometallic nanoparticles, bimetallic nanoparticles have also been used as the substrate in SERS sensing applications[87,88]. Compared to monometallic nanoparticles, bimetallic particles, as either alloyed[89–91] or core-shell[92–96] structures, are found to exhibit enhanced SERS sensing activity. Numerous papers have described the preparation of Au/Ag bimetallic nanostructures[87,89,97,98] and the preparation of Ag/Au bimetallic nanoalloys on Si/SiOx has been demonstrated as a suitable substrate material for the ultrasensitive SERS detection of analytes at low molar concentration[99], whilst Au/Ag bimetallic nanoparticles prepared on the surface of a 3-aminopropyltriethoxysilane (APTES) monolayer modified quartz slide showed an enhanced SERS signal in the presence of 4-aminothiophenol[100]. Like Au and Ag, Pd has also been used for the preparation of bimetallic nanostructures in SERS sensing. For instance 'neuron-like' Au/Pd bimetallic nanoparticles have been used as a substrate material for detection of malachite green, a type of triphenylmethane dye[101], and nanoparticles of an Ag/Pd bimetallic alloy prepared by co-reduction of citrate salts of Ag and Pd have also been used for the SERS detection of 2,6-dimethylphenylisocyanide, 4-nitrobenzenethiol, and 4-ami nobenzenethiol[102]. The use of bimetallic particles with a core-shell structure have been reported to show tunable localized surface plasmon resonance properties by varying the size of the core-metal or by varying the thickness of the shell metal[103,104] and very recently the properties of core-shell nanoparticles and their use in SERS applications have been reviewed and discussed in detail[105]. The effect on the SERS intensity for a *p*-aminothiophenol self-assembled gold nanorod substrate, without and with a silver shell with thicknesses varying between 1 and 4 nm, is shown in **Figure 4b** (corresponding transmission electron microscopy (TEM) and scanning

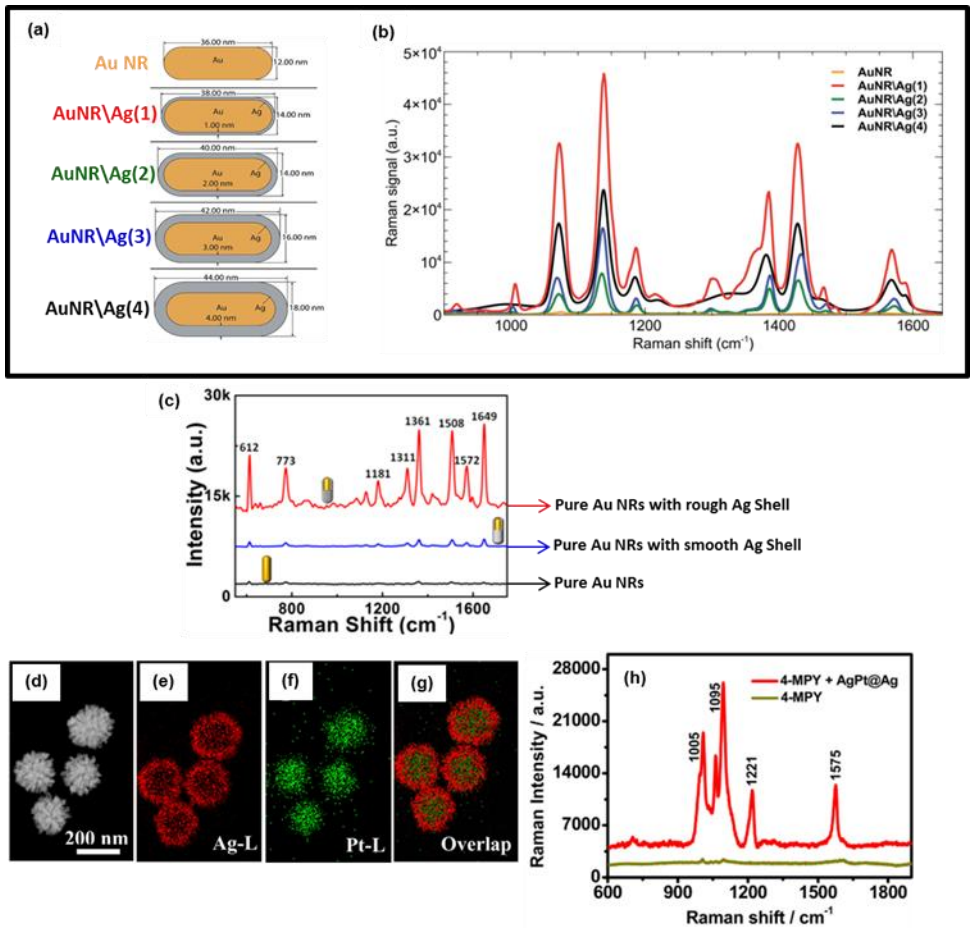

Figure 4. (a) Numerical model representation of Au nanorods with and without Ag shell coverage (1, 2, 3 and 4 nm). (b) SERS spectra measured for all the gold nanorod samples with and without Ag shell coverage in the presence of PTAP (5 μL in 10 mM ethanol) as the analyte molecule. Excitation wavelength – 784 nm (He-Ne laser, 17 mW);. Substrate – microscope glass; (c) Comparative SERS data of Rhodamine 6G (10 μL in 0.1 M ethanol) obtained for monometallic Au nanorods and for Au nanorods with smooth and rough Ag shell. Excitation wavelength – 532 nm (0.12 mW); exposure time – 1 s; Substrate – silicon; (h-k) HAADF-STEM elemental mapping images of Ag-Pt/Ag core-shell nanostructures. (i) Comparison of the SERS spectrum measured for 4-MPY (50 μL in 50 mM ethanol) deposited on substrate made from Au-Pt/Ag nanostructures with the normal Raman spectrum obtained for pure-4-MPY deposited on a glass slide [106–108]; Excitation wavelength – 633 nm;

transmission electron microsopy images (STEM) are shown in **Figure 4a**). Compared to bare gold nanorods, those covered with a silver shell showed increased Raman intensity, with different spectral behavior displayed with varying silver thickness[108]. The use of a thin film composed of nickel-silver core-shell nanoparticles embedded in alumina matrix has also been reported[109].

It is reported that the microstructure of the shell material can also influence the SERS enhancement of the adsorbed chemical molecules for Ag-encapsulated Au nanorods, where it was found that 'rough shell' encapsulated Au nanorods showed a higher calculated enhancement value on adsorption of Rhodamine (1.97×10^8) than found for Au nanorods with a 'smooth shell' (5.12×10^7) or for monometallic Au nanorods (4.02×10^6)[106]. The TEM and STEM images of the bimetallic Au/Ag core-shell superstructures (**Figures 4c and 4f**) and the corresponding high-angle annular dark-field scanning transmission electron microscopy (HAADF-STEM) elemental mapping data are shown in (**Figures 4d-e)**. In other work a bimetallic alloy of Ag/Pt was used as the core material combined with an Ag nanoparticle shell for the SERS detection of 4-mercaptopyridine providing a limit of detection of 0.008 μM[107], and Cu-coated Au nanoparticles prepared on an indium tin oxide (ITO) substrate have shown excellent SERS enhancement although the preparation method was found to be very cumbersome[110]. It is well known that Ag nanoparticles are unstable in ambient conditions and tend to oxidize in acidic environments, and aggregation of Ag and Au nanoparticles in salt solutions leads to precipitation which affects their plasmonic properties during operation. In order to mitigate these problems, metallic nanoparticles can be encapsulated within an insulating or a protective shell. The coverage of the shell not only protects the core material from aggregation but also offers

enhanced stability and surface functionalization. Especially, in the case of SiO_2 coated nanoparticles, the presence of SiO_2 reduces the bulk conductivity of the nanoparticle. Furthermore, it also shields the core material from interference under laser irradiation. In addition to that, an SiO_2 shell is very helpful in preventing the dye molecule from collisional quenching and photo-degradation in the presence of the laser field[111]. It has been observed that during the SERS analysis of Rhodamine 6G detection by Ag@SiO_2 core-shell nanoparticles, the porous silica shell helps to limit the diffusion of dye molecules towards the core structure. This strategy helps to directly quantify the spatial distribution of SERS enhancement when the analyte molecule moved from low to high EM fields inside the dielectric shell[112]. A simple method has been reported for the preparation of Rhodamine conjugated Ag/SiO_2 core-shell nanoparticles using reverse micelle technique in which Igepal CO-520 was used as a surfactant[113] and a cyclic electroplating method was adapted for the preparation of Ag-coated Au/SiO_2 core-shell nanoparticles[114]. Si has also been used for the synthesis of different varieties of Si/M-based (M= Au, Ag, Pd or Pt) core-shell plasmonic structures, where it was suggested that the role of the Si was to minimize unwanted heating effects caused by the metal particles[113]. Similar to SiO_2 and Si, carbon dot nanoparticles (CDNP) were used to encapsulate Ag-nanoparticles, with the as-prepared Ag@CDNP exhibiting strong enhancement for the SERS detection of *p*-aminothiophenol[115].

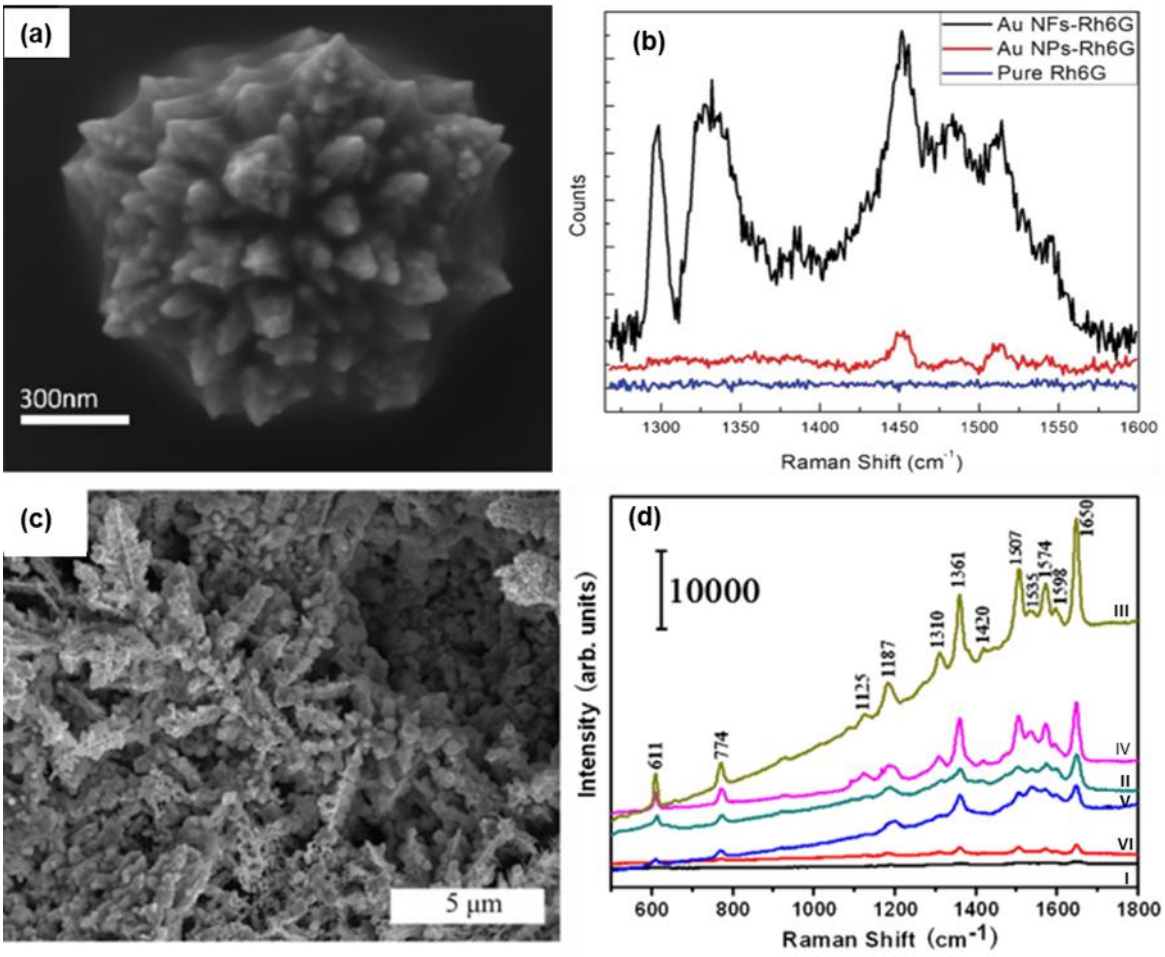

Figure 5. (a) SEM image of gold nanoflowers composed of dendritic gold nanoparticles. (b) Comparison of the SERS sensing data of Au nanoparticles and Au nanoflowers measured in the presence of R6G (5×10^{-5} M)[116] ; Size of Au NFs – 310-820 nm with dendritic tips of size about 310-820 nm; size of Au NPs – 50 to 300 nm; Excitation wavelength – 785 nm; Substrate – glass; (c) Typical SEM image of Au nanodendrite prepared after one stage of MGRR reaction and (d) SERS spectral data obtained for bare Au (I) bare Ag dendrites (II) Au/Ag nanostructures prepared after different stages of MGRR (III) 1 (IV) 3 (V) 5 and (VI) 7 in the presence of 10^{-6} M R6G [148]**.** Excitation wavelength – 514.5 nm; Substrate – copper foil

4.3 Metallic Dendrite Nanostructures

Recently, the use of dendritic nanostructures has been applied in SERS sensing due to their interesting morphology (large number of edge sites for hotspot formation) and large surface area. **Figure 5a** shows the SEM image of gold 'nanoflowers' composed of dendritic nanoparticles which demonstrate signal enhancement for detection of Rhodamine 6G (**Figure 5b**), and Ag/Au bimetallic dendritic structures formed on Si substrates have been used for SERS detection of crystal violet[115]. A multistage galvanic replacement reaction (MGRR) has been used to prepare dendritic Ag/Au (**Figures 5c-d**)[117] and Ag/Pd[118] bimetallic nanostructures for use as SERS substrates, and a 'one-pot' method for synthesis of Ag/Pt dendritic nanoflowers has been demonstrated as a substrate for the detection of 4-nitrothiophenolate (4-NTP) with high sensitivity and good reproducibility[119], attributed to the synergistic effect of the two metals combined with the presence of enriched hot-spots at the sharp corners and edges of the dendritic structures.

Another SERS-based sensor has been developed for the detection of 4-NTP using electrochemically prepared cysteine-directed crystalline Au dendrites on a glassy carbon electrode[120]. In order to enhance the SERS activity, a monolayer of Ag was covered on the surface of gold dendrites using an under-potential deposition (UPD) technique; when compared to pure gold dendrites the silver modified sample showed a three-fold enhancement of the SERS signal at 633 nm. Au/Ag bimetallic dendrites have also shown applicability towards 4-mercaptopyridine (4-MP) sensing[121].

4.4 Semiconducting Nanostructured Metal Oxides

Due to their enriched surface property, high chemical and thermal stability, nanostructured semiconducting metal oxides (NSMOs) find potential interest in many fields including chemical sensors[122], photovoltaics[123], optoelectronics[124], and energy storage and conversion[125–128]. NSMOs have also been extensively employed as the active substrate material in SERS applications, and are particularly attractive due to their low cost and high stability[129–131]. However, enhancement of the Raman signal is found to be low compared to that found for noble metals because the increase is due to chemical enhancement rather than the EM enhancement mechanism found with metals. Despite this, a variety of NSMOs such as NiO, Cu_2O, CuO, ZnO, TiO_2, α-Fe_2O_3, Fe_3O_4 have been found to shown significant SERS activity. NiO[132] and TiO_2[133] NSMOs have been demonstrated to provide SERS enhancement on adsorption of pyridine, with a different excitation profile found to that obtained when using monometallic metals such as Ag, Au, Ni, Pd, Ti and Co.

The lower enhancement factor found for NSMOs has been overcome by incorporating the NSMOs with noble metal nanoparticles. For instance Ag nanoparticle modified NiO nanoflakes have been used as a substrate for the SERS detection of polychlorinated biphenyls, exhibiting a very low detection limit of 5 μM[134]. Among the various NSMOs, titanium oxide (TiO_2) has been widely used in SERS. In most of the reports bare TiO_2 provides a very small SERS enhancement, however in combination with Ag or Au nanoparticles it is found to provide a much larger enhancement in the SERS intensity and very recently a review has been published exclusively on the application of noble metal-TiO_2 nanocomposites in SERS investigation[135].

An example is for the SERS sensing of 4-mercaptopyridine where Ag-nanoparticle coated TiO_2 nanofibers exhibited a very high enhancement factor (**Figure 6**).[136]

ZnO is also of interest for the development of SERS substrates because it offers strong light confinement due to its high refractive index value which helps in enhancing the SERS signal[137], with nanostructured ZnO having been prepared with morphologies such as nanospheres, nanowires, nanorods, nanocones, nanoneedles and nanobelts[138–143]. Recently, the application of various ZnO-based materials as SERS substrates has been reviewed and two methods emphasized for improving the enhancement obtained; (1) heavy element doping, and (2) preparing composites of nano-ZnO with noble metals[144]. Many reports have shown significant enhancement in the SERS intensity by using composites of ZnO with Au or Ag nanoparticles[145–148]. The effect on the enhancement of SERS intensity of the ZnO nanoparticle morphology in nanocomposites with noble metals has also been studied[145,147,149], with ZnO nanorods and nanotubes shown to give a very large SERS intensity. This was attributed to a higher number density of metal nanoparticles on the surface of these structures due to their high specific surface area, leading to the generation of 3D plasmon hotspots and consequently large SERS enhancement even at very low concentration. Additionally, ZnO nanostructures with a high surface area offer a greater number of sites for adsorption of analyte molecules[150]. This has been observed for Ag-nanoparticle decorated ZnO nanowires (**Figure 7**), which showed a very high Raman enhancement value of up to 10^{10} in the presence of Rhodamine 6G at a concentration 10^{-10} M[151]. Metallic copper substrates have previously been utilized as SERS substrates[152–154], however, in 1998 the SERS spectra of pyridine molecules adsorbed on copper(I) oxide (Cu_2O) substrates were demonstrated and compared with the spectra obtained for a pure Cu substrate[155].

Like Cu_2O, copper(II) oxide (CuO) has also been investigated in SERS studies[156–158]. Very recently, a substrate made from composites comprised of CuO nanowires and Cu_2O nanostructures (**Figure 8a-f**) has been investigated for the SERS detection of 4-methylbenzenethiol[159]. Another interesting phenomenon in this experimental study was the demonstration of self-cleaning behavior of the SERS substrate using photo-catalytic degradation under visible light illumination (**Figure 8g**), which improved the reusability of the substrate materials with more than 85 % of the original SERS activity preserved even after 7 cycles of measurements (**Figure 8h-i**). In general, excellent recyclability for composites of NSMOs with noble metal nanoparticles such as TiO_2-Au, ZnO-Ag, and Ag-TiO_2, has been demonstrated after photocatalytic cleaning treatment[160–162].

Nanostructured iron oxide has also been investigated as a substrate material to enhance SERS signal. A preliminary study on the SERS effect of thin films of iron oxides was reported when SERS was used as a spectroscopic tool to analyze the passivation behavior of iron oxide thin films during electrochemical reduction[163], and hematite monolayer-modified quartz substrates have been used for SERS sensing of 4-mercaptopyridine (4-MCP)[163]. Both the hematite and maghemite phases of iron oxide (α-Fe_2O_3 & γ-Fe_2O_3) have been investigated as substrates for enhancing the signal intensity[164–167]. Magnetite (Fe_3O_4) has also been employed to improve the performance of SERS sensors[168–172] and very recently the application of magnetite nanoparticles in SERS sensing has been reviewed[173].

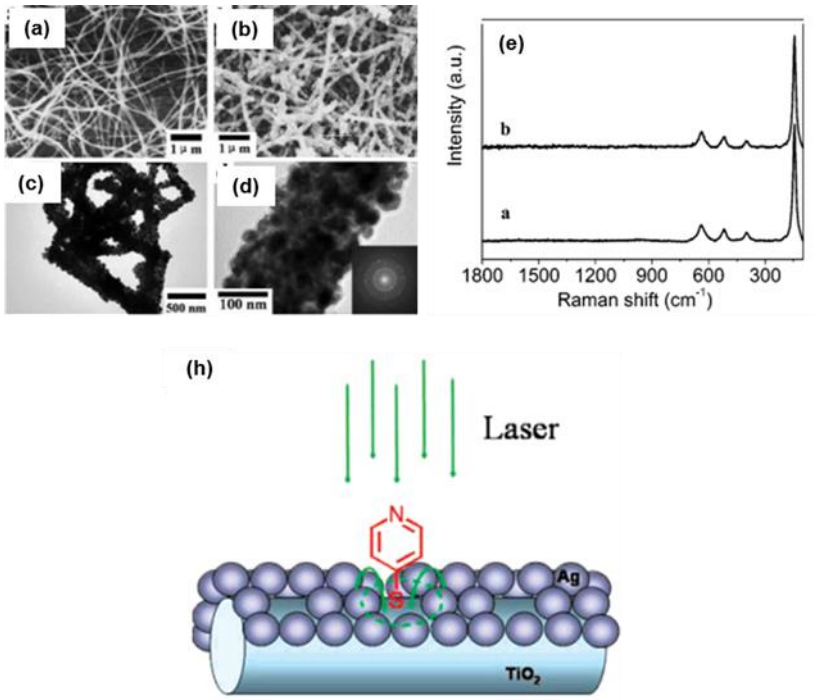

Figure 6. (a-d) SEM and TEM images of pure and Ag nanoparticles coated TiO_2 nanofibers (e) SERS spectra measured for substrate made from pure and Ag nanoparticles coated TiO_2 nanofibers in the presence of 4-Mpy (0.1 M). (f) Illustration showing the SERS sensing mechanism of Ag coated TiO_2 nanofibers under laser excitation. [136] Excitation wavelength – 514.5 nm; substrate- glass slide

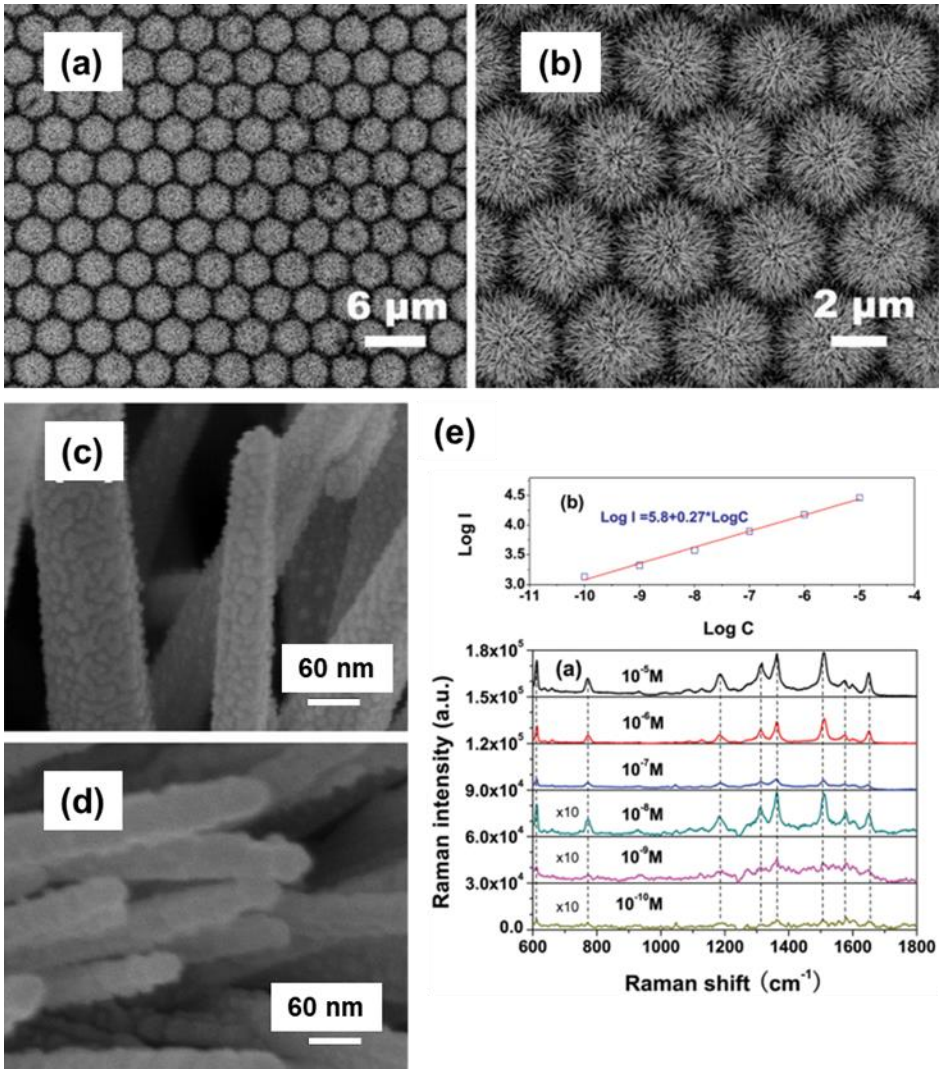

Figure 7. (a,b) SEM images of ZnO nanoflowers measured at two different magnifications. (c,d) SEM images showing Ag coating on individual ZnO nanorods (e) SERS spectral data and log-log plot measured for ZnO nanoflowers at different concentrations of R6G (10^{-5} – 10^{-10} M). [151] Excitation wavelength – 532 nm; substrate- patterned sapphire

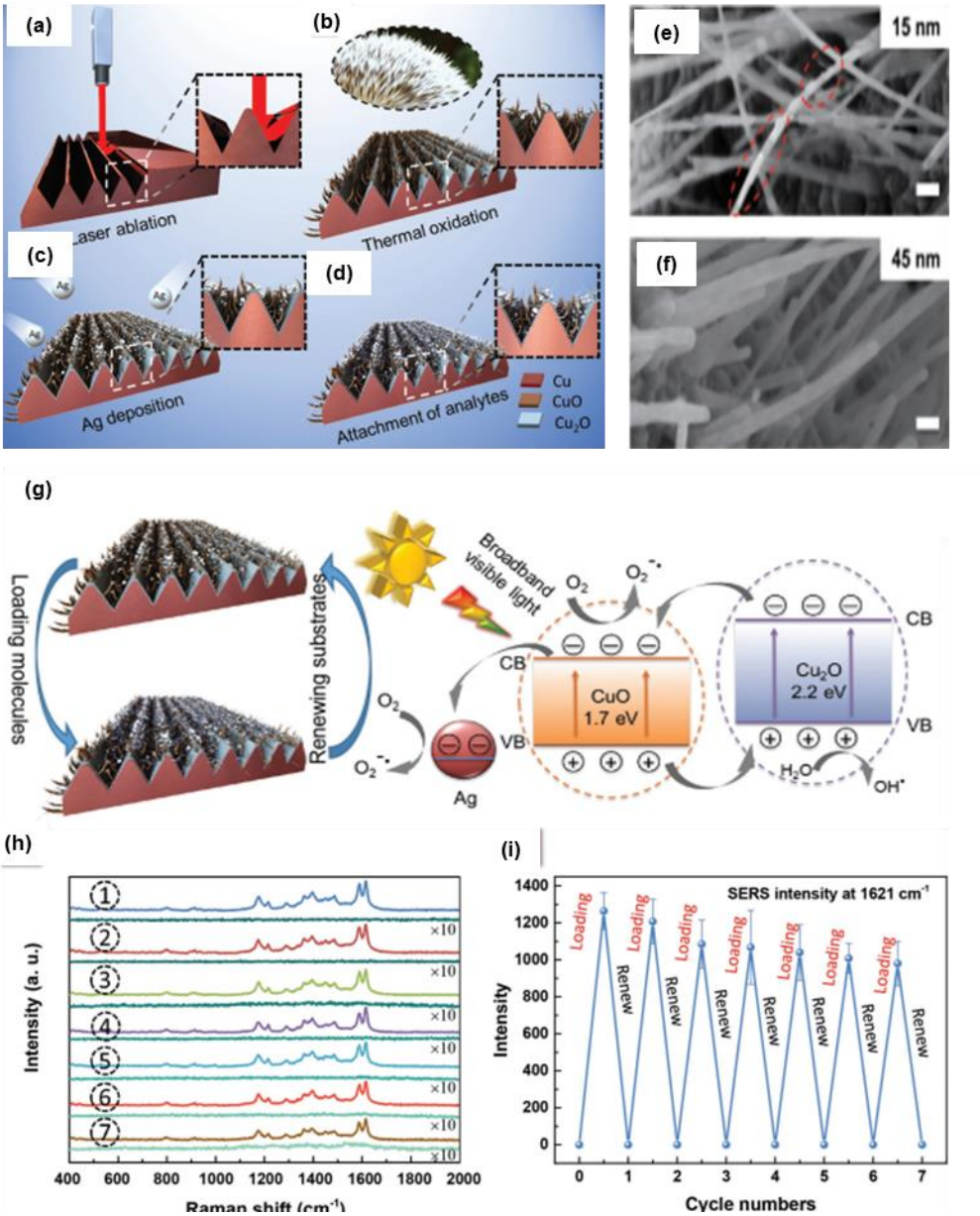

Figure 8. (a-d) Schematic illustration showing the fabrication of binary CuO-Cu_2O composite based SERS substrate on Cu sheet. (e,f) SEM images of Ag doped CuO nanowires. (g) Schematic diagram showing the self-cleaning photocatalytic degradation process. (h,i) SERS spectra of Ag/CuO NWs/Cu_2O composite sample in the presence of malachite green before and after self-cleaning treatment to check reusability and their corresponding intensity data measured at a band value of 1621 cm^{-1} [174]. Excitation wavelength – 514 nm; Substrate- Cu sheet

4.5 Metal Oxide-based Nanocomposites

In the last few decades, significant enhancement in SERS intensity has been achieved by employing nanocomposites consisting of metal nanoparticles and nanostructured metal oxides. Most of the SERS substrates made of pure noble metal nanoparticles are found to show excellent sensitivity towards various analyte molecules. Although pure metallic nanoparticles have shown effective enhancement, they have also exhibited poor stability due to oxidation in air or aggregation in saline solutions. In addition, factors such as temperature, time and chemical environment also influence the stability of the metallic nanoparticle based SERS substrates. For instance, it has been shown that thermal energy (either from Raman measurement or probe temperature) degrades the SERS substrates over time resulting in low sensitivity towards analyte molecules[175,176]. Nanocomposites with metal oxides and noble metal particles show very large SERS intensity, for instance nanocomposites of metal oxides including CuO, Cu_2O, ZnO, and TiO_2 with Au or Ag nanoparticles[177–180], with improved stability compared to single noble metals owing to a synergistic effect of noble metal component and the metal oxide support resulting from a charge transfer process between the noble metal and adsorbed molecules and at the interface between the noble metal and the metal oxide nanostructures. In general, EM enhancement is solely responsible for the SERS enhancement. However, in the case of noble metal-metal oxide hybrids, the presence of noble metal nanostructures in the vicinity of metal oxide can also enhance the SERS performance to some level due to the additional CE between the metal and adsorbed molecules.[181] W. Ren *et al.* have reported the synthesis and application of Au-TiO_2 core-shell nanocomposites towards SERS sensing of trichloroethylene (TCE) in water medium[182], in which it was observed that the TCE molecules were oxidized due to the

photocatalytic nature of TiO_2, forming HCl. The interesting observation in their study is that they used the SERS intensity corresponding to the concentration of the HCl byproduct to calculate the concentration of the TCE analyte. SERS substrates composed of Ag nanoparticle-decorated TiO_2 'nanograss' have been used for the highly efficient detection of R6G and 4-ATP molecules [183]. The developed SERS substrate was found to be easily self—cleanable and reactivated under visible light. Y. Zhao *et al.* reported the preparation of TiO_2 nanobelt decorated with Ag nanoparticles by an electroless plating method[184], with the TiO_2/Ag nanocomposites showing high SERS sensitivity towards various molecules such as 4-MBA, R6G and 4-ATP and excellent self-cleaning properties under UV irradiation. Like TiO_2, a hydrothermally synthesized hybrid structure composed of 3D hierarchical ZnO decorated with Ag nanoparticles has been employed for the SERS detection of various organic pollutants viz. rhodamine 6G (R6G), Nile blue A (NBA), 4-chlorophenol (4-CP) and 2,4-dichlorophenoxyacetic acid[185]. The ZnO-Ag hybrids showed high sensitivity towards R6G and 4-CP with very low LOD value of 1×10^{-13} M and 5×10^{-9} M respectively. Furthermore, because of the good stability of the ZnO-Ag hybrids, the developed SERS substrate was easily self-cleaned under UV radiation. Magnetite based nanocomposites with Ag and Au nanoparticles have been successfully employed for the SERS detection of neurotransmitter dopamine and food colours such as acid orange II or brilliant blue[185–187].

5 2D inorganic Nanomaterials for Sensing

Investigations on the development of SERS sensitivity and specificity have confirmed the importance of maximizing hot-spots (EM enhancement) and enhancing the polarizability of the probe molecule by surfaces sites (chemical enhancement) for improved performance in SERS

sensing. For example, highly surface-roughened Ag-nanoplates (3D morphology) provide a high density of hot-spots due to the number of surface sites, and sharp edges of the nanoplates [188]. Whilst these rough metal surfaces induce a strong local EM field, alignment of the Fermi level at the metal surface and lowest unoccupied molecular orbital (LUMO) energy of the probe molecule is non-optimal for chemical (CM) enhancement. The maximum signal enhancement requires a combined effect of both polarization due to charge transfer (CM enhancement), and excitation of surface plasmons (EM enhancement).

Excellent reviews on Raman scattering of 2D materials [189,190] have emphasized the importance of features such as edges, in-plane symmetry, defects, stacking, doping and charge interactions in contributing towards the unique properties of these materials. In surface functionalized 2D materials a significant suppression of the background flourescence signals are observed compared to pristine substrates. This is because surface modification creates stronger interaction between the 2D materials and the analyte molecules, resulting in enhanced Raman intensity. For instance, plasma treated MoS_2 showed enhanced SERS performance with very high suppression of background signals, attributed to the formation of surface defects caused by the introduction of gaseous species[191]. There is another report in which. Z. Zheng *et al* found that annealing (oxidation) temperature plays an important role in the suppression of background signals of 2D materials, with MoS_2 annealed at temperatures below 400 ° C having a lower flourescence background, which was ascribed to the generation of more free oxygen carriers at low temperature[192]. The number of layers in the 2D material also determines the suppression of the background fluorescence signal, with S. Jin *et al* showing that a monolayer 1T-MoS_2 sample showed an enhanced Raman signal without flourescence background for R6G probe molecules,

compared to multilayer 2H-MoS_2.[193]. In the following sections, we summarise the impact of 2D materials and 2D transition metal chalcogenides (2D TMCs) and their progress in SERS sensing.

5.1 Graphene

The layered honeycomb-like arrangement of sp^2 bonded carbon atoms of graphene, providing high π electron density at the surface, a chemically inert surface, flexibility and biocompatibility, have made graphene-based surface-enhanced Raman scattering (G-SERS)[194] a hot topic.[195] In G-SERS, the interaction of π electrons, vibrational coupling, and the effect of the HOMO and LUMO of the probe molecules on the Fermi level of graphene enhances the Raman signal.[196–198] An investigation of a 2D graphene monolayer using the probe molecules phthalocyanine (Pc), Rhodamine 6G (R6G), protoporphyrin IX (PPP) and crystal violet (CV), exhibited an enhanced Raman signal for Pc and PPP.[195] Both Pc and PPP are conjugated and macrocyclic structures similar and parallel to the graphene surface and which therefore induce better charge transfer due to π-π stacking bond formation, and Fermi level and vibrational coupling.[195] Indeed, this phenomenon was confirmed with studies on SERS enhancement for different molecular orientations of copper phthalocyanine (CuPc) on a graphene layer.[199] Specific molecular orientation of the probe molecule adsorbed onto the graphene surface can promote charge transfer and hence enhance the interfacial dipole and polarizability.[199,200] The D_{4h} symmetry molecule (CuPc) has macrocycle- and isoindole ring-related vibrations which enhance the π-π interactions between CuPc and graphene for electron transition, polarizability, and Raman scattering cross-section when in a lying-down orientation, rather than upstanding (**Figure 9a**),[199] because the dipole moment of the molecule effectively shifts the energy levels of graphene and results in an enhanced Raman signal (**Figure 9b**).[201] The high dipole moment of a tricyanofuran

group (TCFP) (23.3) exhibited an enhanced Raman signal due to strong interfacial coupling between the highly polarizable molecule and 2D-graphene. **Figure 10**, demonstrate the relationship between the molecular configuration of the probe molecule and the graphene surface.[196] The interaction of protoporphyrin IX (PPP) with graphene via its hydrophobic functional group (-CH=CH_2) face gave stronger signal enhancement than via the hydrophilic face (-COOH), while for a CuPc molecule, no variation in the Raman signal according to the binding mode. This showed that the more chemically similar group led to an increased degree of charge transfer and increased polarizability tensor and increasing the Raman scattering cross-section. The molecular selection rules for the enhancement factor dictate the energy levels and symmetry of the molecule must match the surface of the Raman substrate [198]. The investigation of probe molecules has been carried out in two different ways (1) similar molecular structure with different energy levels, and (2) similar energy levels with different molecular structure [198]. The strength of molecule-surface interactions, molecular orientation, and the dipole moment of the molecule, has been a criterion for a molecule to be considered for enhancement factor.

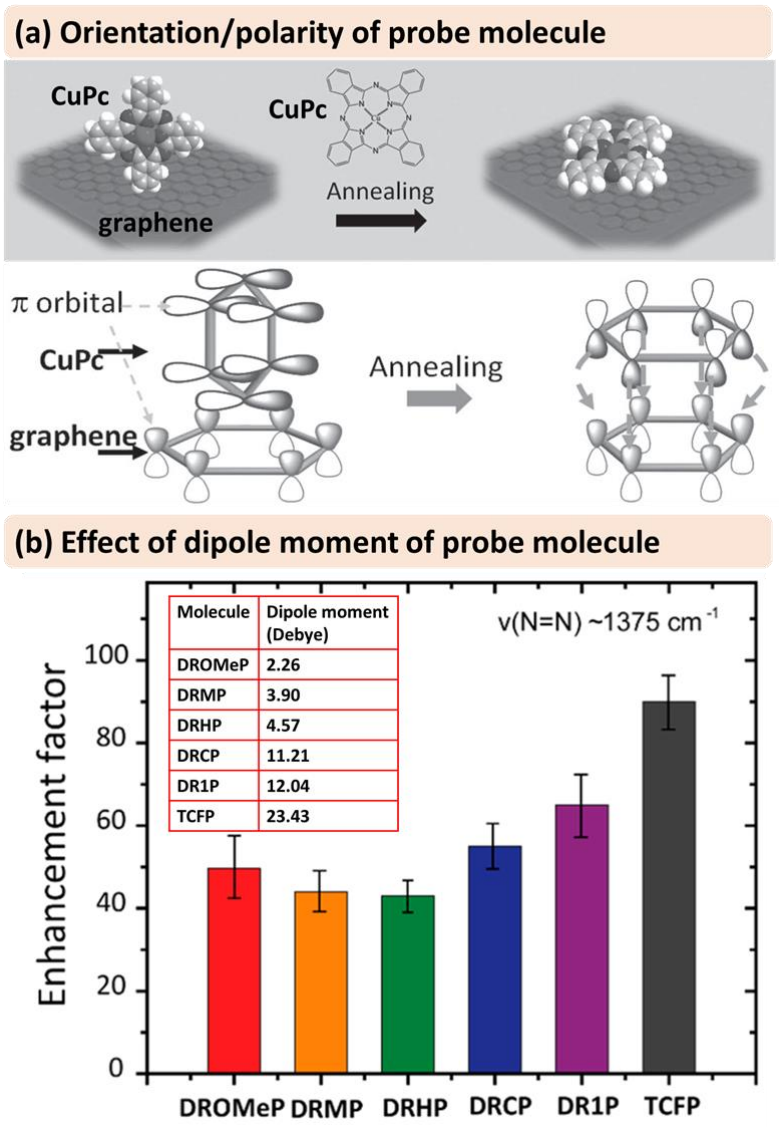

Figure 9. (**a**) Schematic illustration of molecular orientation and the relative direction of the delocalized π orbital of graphene and the CuPc molecule before and after annealing [199]. (**b**) Raman enhancement factor of the ν(N=N) mode of different chromophores on graphene. (pyrene-tethered azobenzene chromophores with different tail groups at the para position of the benzene ring terminating the azobenzene, namely: methoxy (DROMeP), methyl (DRMP), hydrogen (DRCP), nitrile (DRHP), nitro (DRIP and tricyanofural froup (TCFP))[201]. Excitation wavelength – 514.5 nm; Substrate- SiO_2/Si

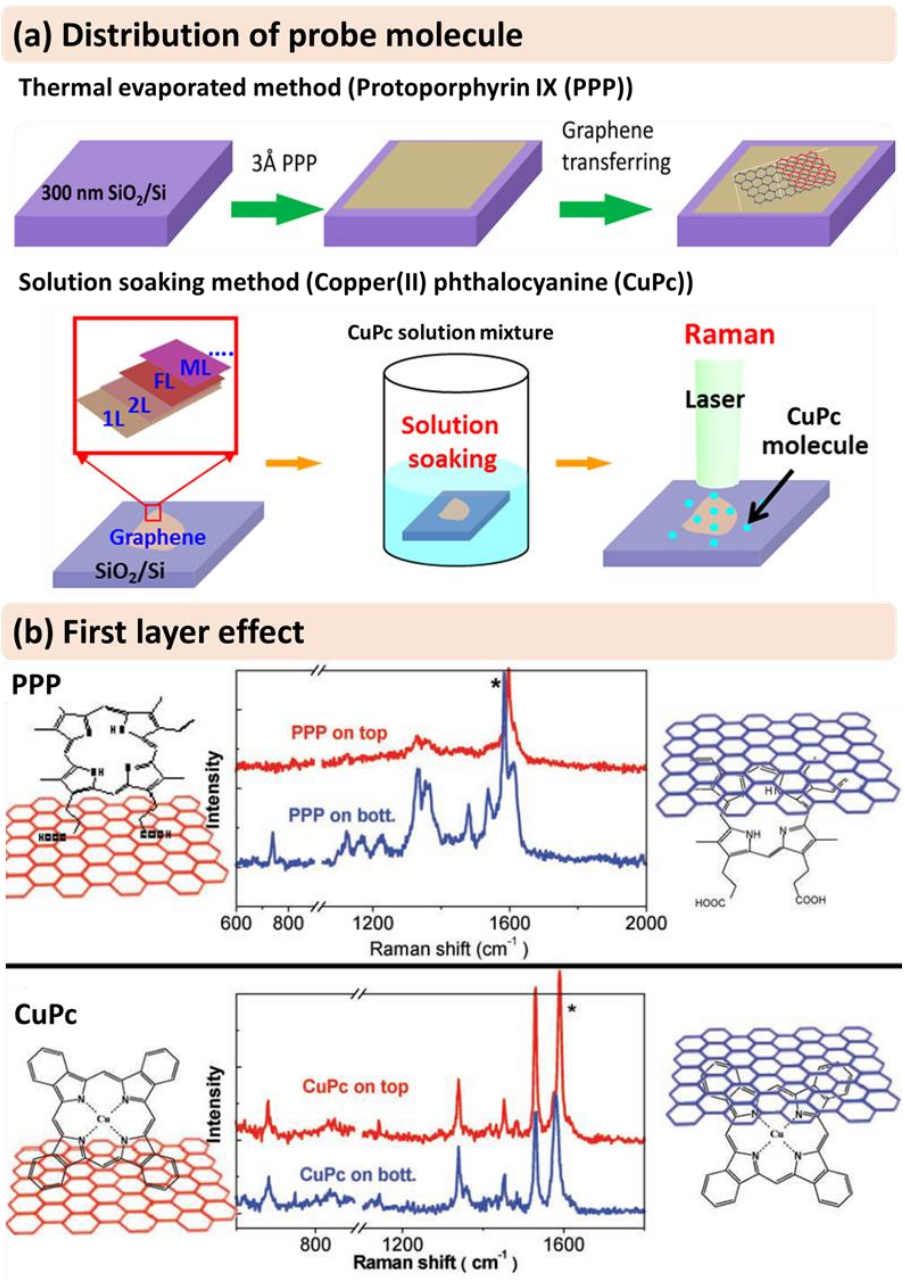

Figure 10. (a) Schematic illustration of the preparation of the sample by solution soaking method (CuPc) and thermally evaporated (PPP)[202]. **(b)** Raman spectra of PPP and CuPc molecule on top and bottom of graphene layer and its corresponding molecular configuration. (* - G-band of graphene, red line represent the top position of molecule and blue line represent the bottom position of molecule) [196]. Excitation wavelength – 514.5 nm; Substrate- SiO_2/Si

Graphene monolayers ensure the highest enhancement factor, with increasing the number of layers gradually decreasing the Raman signal. This problem was identified by a detailed investigation on the deposition of molecules and the impact of the number of graphene layers on the energy band.[202] The deposition of equal molecule density on 1 – 6 graphene layers using thermal deposition method exhibited a uniform adsorption of probe molecules (**Figure 10a**), with monolayer and bilayer graphene having a different match to the adsorption of probe molecules energy (**Figure 11a**). This demonstrated the impact of equal molecule density and energy band structure in SERS sensing. However, Lin *et al.* [203] showed that for anisotropic surfaces like black phosphorous (BP) or rhenium disulphide (ReS_2), an enhancement of the Raman signal can be obtained even when probe molecules are distributed non-uniformly. Furthermore, to prove an anisotropic Raman enhancement effect Wu *et al.*[204] confirmed the polarization dependent charge transfer between anisotropic single-walled nanotube arrays and organic molecules.

In order to improve CM-enhancement, surface functionalization (**Figure 11b-c**) through metal decoration, non-metal decoration, surface passivation, and fluorescence quenching, has been reported.[194,205,206] As well as the role of the substrate material and probe molecule on the enhancement factor, the incident radiation also modulates the Raman scattering effectively by self-absorption of the molecule and electron-phonon coupling [207–209]. For example, **Figure 11c** depicts the resonant excitation of Nile Blue A (NBA) was larger, with stronger charge transfer and Raman scattering intensity, when using a 633 nm laser than when using a 514 nm laser [209].

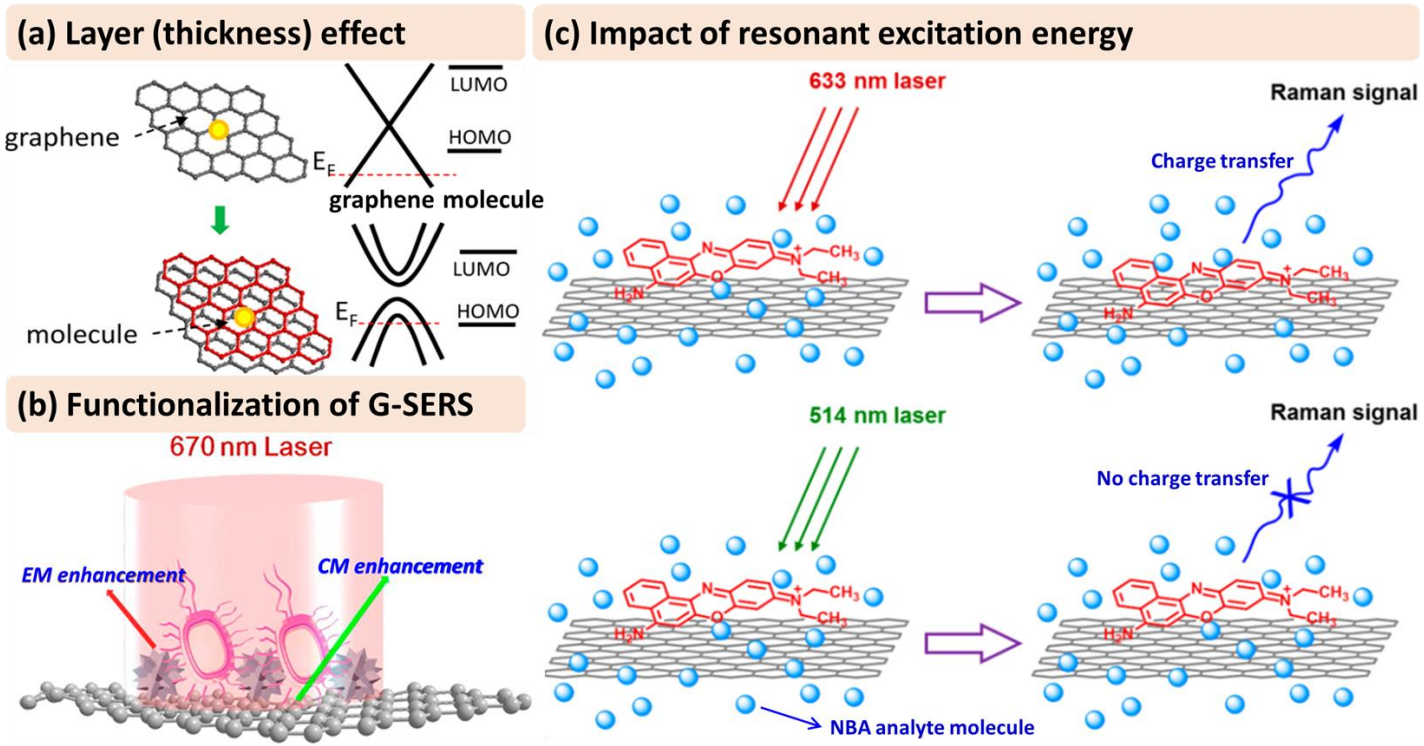

Figure 11. Schematic representation of **(a)** the mono- and bi-layer graphene and its energy band structure with energy level of probe molecules [202]; **(b)** the hybrid graphene oxide-based SERS probe for tuning electromagnetic and chemical enhancement simultaneously to detect methicillin-resistant *Staphylococcus aureus* (MRSA) bacteria [210]. **(c)** The Raman signal enhancement of nile blue A (NBA) under resonant (633 nm) and non-resonant (514 nm) excitation [209].

High-quality 'ultra-clean' graphene quantum dots (GQD) prepared using a plasma-enhanced (PE-) chemical vapor deposition method (2.2 nm, P-GQD-1, **Figure 12a**; 6.2 nm, P-GQD-2, **Figure 12b**) exhibited a size-dependent enhancement factor increase and selective probe molecule recognition.[211] The Raman spectra of thermally evaporated R6G (**Figure 12c**) and CuPc (**Figure 12d**) demonstrated the improved Raman enhancement efficiency of P-GQDs compared to graphene or quantum dots prepared by other methods. The high crystallization, low defect density, atomically clean surface and accessible edges of the graphene quantum dots (GQDs) favoured such efficiency. Furthermore, the calculated energy alignments between the orbitals of P-GQDs and the target molecules were in alignment, to provide a higher charge transfer integral (**Figure 12e-h**).

Although 2D graphene possesses excellent properties for SERS analysis such as clean signal, stable response, transparency, flexibility, and recyclability[194,205], there are still many challenges remaining for further development ,such as the optimization of charge transfer for maximum chemical enhancement, the spectral fluctuation for molecular-level detection, the photocarbonisation of molecules, the specific detection of particular probe molecules and reliable real-time application. In this context, other 2D materials such as hexagonal boron nitride (h-BN), orthorhombic black phosphorus (BP), molybdenum disulphide (MoS_2), triclinic rhenium disulphide (ReS_2), gallium selenide (GaSe), tungsten diselenide (WSe_2), tungsten telluride (WTe_2) and titanium carbide (TiC) have been investigated to address the challenges. For example, the stable phase of 1T-WTe_2 exhibited an ultra-low detection (femtomolar level concentration) towards R6G with promising aging stability[212], demonstrating that 2D layered materials are a feasible SERS material for real-time applications.

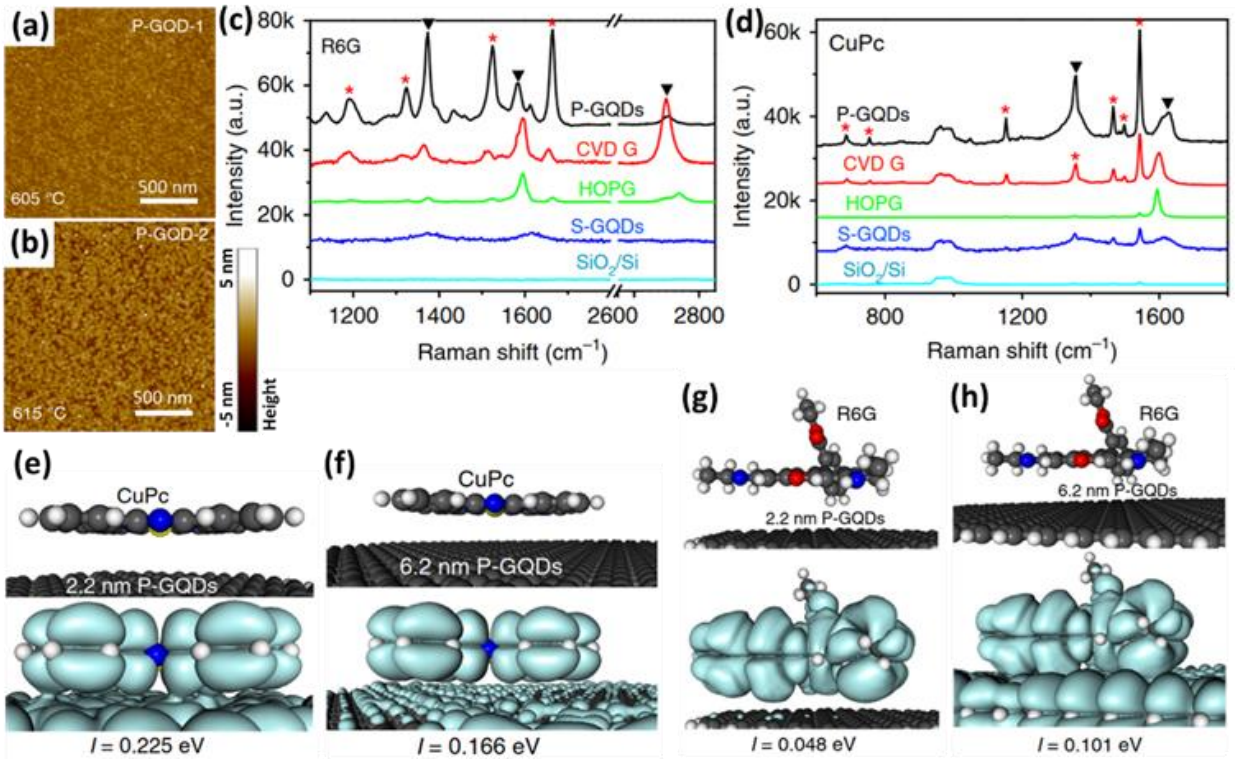

Figure 12. (**a-b)** Atomic force microscope (AFM) images of plasma-enhanced chemical vapor deposition grown graphene quantum dots at 605 °C and 615 °C respectively. (**c-d)** Raman spectra of thermally evaporated rhodamine 6G (R6G), and copper phthalocyanine (CuPc) on SiO2/Si, graphene, quantum dots produced by solution processes (S-GQDs), HOPG, transferred chemical vapor deposition (CVD) graphene and P-GQDs respectively. Excitation wavelength – 532 nm ; Concentration of R6G and CuPc- 0.2 n m thick layer on the substrate. **(e-h)** The calculated molecular orbital (at the HOMO level of CuPc and R6G) densities of CuPc/P-GQD-1, CuPc/P-GQD-2, R6G/P-GQD-1 and R6G/P-GQD-2 respectively. (**e-h)** The atomic models used in the density functional theory (DFT) calculations and the calculated charge transfer integrals respectively. [211]

5.2 Boron nitride

Atomically thin hexagonal boron nitride (h-BN) is free of dangling bonds and charge traps, has large optical phonon modes, and a large electrical band gap (5.97 eV)[213–215], which strongly favors its potential use as a SERS substrate. The hexagonal structure with a bond length of 1.44 Å is similar to that of graphene, while its polar surface with high resistance to oxidation led to its consideration as an alternative to 2D graphene for Raman signal enhancement[214,216]. The CuPc probe molecule on 2D graphene (zero-band gap and non-polar C-C) and h-BN (wide-band gap and strongly polarised B-N bond) exhibited different enhancement mechanisms (**Figure 13a**)[23]. The strong interface dipole interaction between CuPc and polar, insulating h-BN enhanced the resonance Raman scattering at the lower frequency phonon modes of CuPc (682, 749, 1142, 1185 cm^{-1}), whilst in contrast, non-polar and metallic graphene exhibited charge transfer between CuPc and graphene at higher frequency vibrational modes (1342, 1452, 1531 cm^{-1}).

We have previously seen that increasing the number of graphene layers led to non-uniform charge distribution which affects the distribution of CuPc on the substrate[202]. However, the Raman intensity of CuPc coated on different thicknesses of h-BN flakes exhibited a uniform distribution of intensity confirming the interface dipole interaction of symmetry-related perturbation (**Figure 13b**)[23]. Furthermore, the Raman frequency of mono- and few-layer h-BN demonstrated the thickness independence of the intrinsic E_{2g} mode of h-BN (**Figure 13c-e**).[217] Towards the sensing of R6G molecules, atomically thin BN showed high intensity Raman signals than that of bulk BN.[218] Although, BN layer with different thicknesses exhibited similar dipole interaction with same magnitude of chemical enhancement[23], the observed high intensity SERS signal towards R6G molecules revealing the stronger adsorption capability of atomically

thin BN than the bulker one[218]. This specific strong adsorption property might make h-BN, as a less favorable for SERS application. However, due to its high thermal stability characteristics (800 °C), it can be utilized as a reusable coating on noble metal layers for Raman enhancement.[218–221] Also, h-BN functioned as a protective barrier (insulating layer) to avoid the photocatalytic reactions of organic molecules and oxidation of the SERS material. **Figure 13f** [221] depicts the impact of photocatalytic reactions on Au/SiO_2 and h-BN/Au/SiO_2 SERS materials. The h-BN protective layer prevents the formation of Au oxides and oxidation of 4-Aminobenzenethiol due to the photo-induced reactions. Similarly, the strong adsorption capability of h-BN layers were confirmed as a critical feature when used as a hybrid SERS material. In **Figure 13g**[221] the high adsorption of benzo(α)pyrene on h-BN covered Au/SiO_2 SERS material, due to π-π interactions, demonstrated its potential for chemical stability.

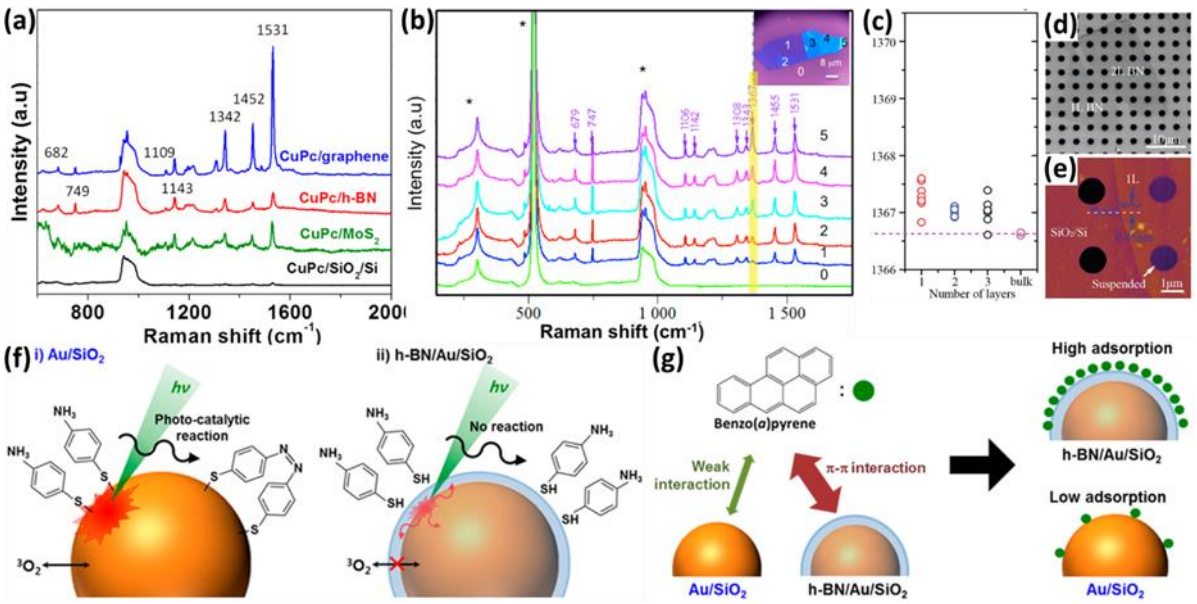

Figure 13. (a) Raman spectra of the CuPc molecule on the blank SiO_2/Si substrate (black line), on graphene (blue line), on h-BN (red line), and on MoS_2 (green line) substrates. (The Raman signal was excited by a 632.8 nm laser and peaks frequencies of the Raman signals from the CuPc molecule are marked and the baseline correction was removed.) [23]; thickness of the CuPc molecule on all the substrates – 2 Å **(b).** The Raman enhancement effect on h-BN flakes of different thickness of h-BN. The numbers 0 -5 in the inset and labels correspond to the position of Raman spectra. "*" - peaks from the SiO_2/Si substrate. The yellow shadow shows the location of the 1367 cm^{-1} Raman mode from h-BN [23]. **(c-e).** Raman frequencies of the G band of suspended 1-3L BN and bulk h-BN, Optical image of 1-2L BN nanosheets partially suspended over ~1.3 μm wells, and The corresponding AFM image with height trace inserted respectively [217]. **(f-g).** Schematic mechanism to explain photocatalytic reaction and adsorption of benzo(α)pyrene on h-BN/Au/SiO_2 substrates respectively [221].

5.3 Black phosphorous

The layered black phosphorous (BP) puckered honeycomb structure (**Figure 14a-b**), stacked together by van der Waals interactions, exhibits a narrow band gap (0.3 eV in bulk), strong in-plane symmetry, anisotropic charge carrier mobility, and unique angle-dependent properties.[222–225] Both electrons and photo-excited excitons in BP follow the armchair (AC) direction compared to the zigzag (ZZ) direction due to the lower effective mass.[203,225] This characteristic feature is apparent in the anisotropic Raman enhancement for layered BP substrates. This behavior was confirmed through the study of the interaction of CuPc molecules on BP and graphene layers.[203] The uniform distribution of charges in BP layers redistributed into one-dimensional AC directions after interaction with CuPc probe molecules (**Figure 14c**), but in graphene the uniform charge distribution remained the same, even after interaction of CuPc (**Figure 14d**). In general, molecular orientation of probe molecules is important for the enhancement of SERS intensity. In the case of BP substrate, the high mobility charge carriers and anisotropic excitons towards AC direction favored the charge transfer process between CuPc molecules and substrates irrespective of the molecular orientaion (**Figure 14c,d**). This specific anisotropic charge distribution benefits the measurement of probe molecules irrespective of distribution on the substrate showing the highest enhancement factor for a single CuPc molecule. However, although the overall enhancement factor for CuPc is low the advantage of the specific path of carriers and enhancement of the Raman signal for randomly distributed or low concentrations requires further investigation.

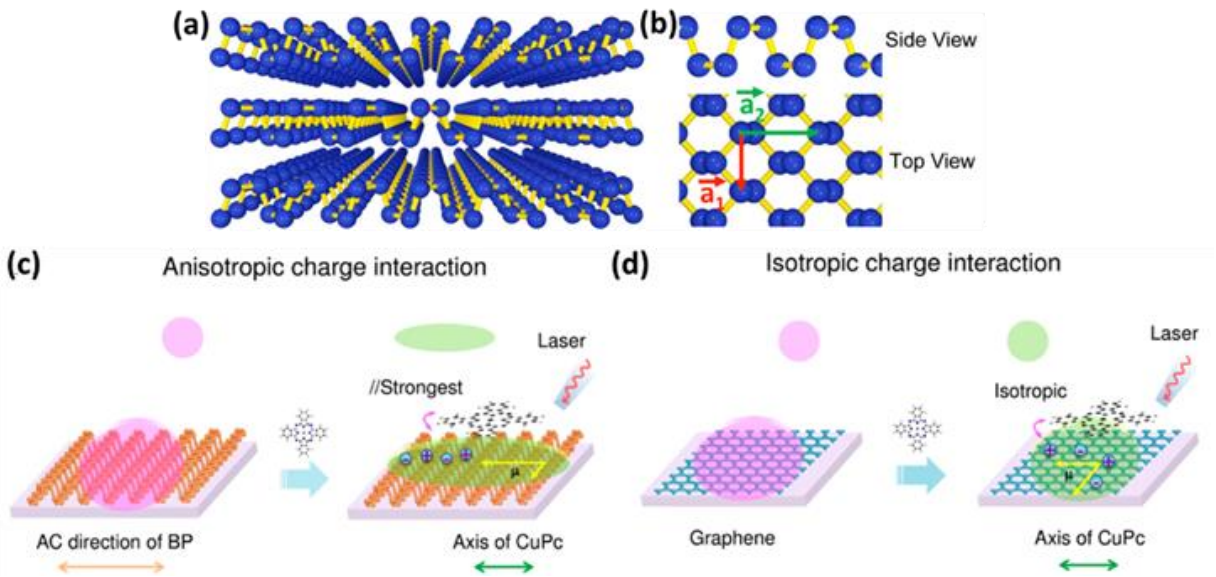

Figure 14. Puckered honey comb layered crystal structure of black phosphorus **(a)** lateral view of few-layer, **(b)** side view and top view of monolayer.[226] **(c, d)** Schematic illustration of anisotropic and isotropic charge interaction processes in **(c)** CuPc/BP and **(d)** CuPc/graphene respectively.

5.4 MXenes

MXenes are 2D materials composed of transition metal carbides and nitrides (carbonitrides) with general formula $M_{n+1}X_nT_x$ (n=1-3), where M is an early transition metal, X is a carbon or nitrogen, and T_x is surface terminated functional group[227,228]. Their metallic conductivity and hydrophilic terminated surfaces (-OH, -F, -O) make these promising materials in biosensing[228]. A spray-coated $Ti_3C_2T_x$ layered substrate showed an enhancement factor of ~1.2×10^6 for R6G (488 nm laser)[229], and the Raman intensity mapping demonstrated the contribution of hot-spots towards the enhancement. The $Ti_3C_2T_x$ layers displayed good SERS performance towards other molecules including methylene blue (MB), crystal violet (CV) and acid blue (AB). The MB cationic charged dye exhibited good adsorption on the substrate due to the negatively charged (-OH terminated functional group) surface. The mutual process of hot-spot formation due to inter-band transition to the vacant energy states of the functional group and charge transfer to the probe molecule provided a synergistic enhancement of both electrical field enhancement and chemical enhancement (**Figure 15a**). The development of 'hot-spots' on the $Ti_3C_2T_x$ flakes was witnessed by the observation of transverse oscillation (centered at ~620 nm) and longitudinal oscillation (centered at ~780 nm) due to the inter-band transitions and geometry. [229]

The 2D-transition metal nitride Ti_2NT_x exhibited a SERS enhancement factor of 10^{12} towards an R6G probe molecule.[230] The high electron density concentration at the N atom and high surface area of Ti_2NT_x led to the interaction of the probe molecule and transfer of electrons from the Ti atoms. An important potential advantage of MXenes is the ability to deposit the material on different substrates, including flexible materials. **Figure 15b** displays the fabrication of MXenes on paper, silicon, and glass substrates. Interestingly, Ti_2NT_x on the paper-based

substrate showed detection of the femtomolar concentration of R6G with the highest efficiency (enhancement factor of 10^{12}). FESEM images of Ti_2NT_x deposited on glass/silicon (**Figure 15c**) and paper (**Figure 15d**) substrates demonstrated the variation in surface roughness and surface area of flakes. The MXene flakes on paper-based substrates had the higher surface area and therefore had the highest enhancement factor. The investigation on MXene materials for SERS applications is at an early stage. Till date, more than twenty different compositions of MXenes have been experimentally prepared and [228] with the possibility of functionalization with different terminal groups, MXene materials will become an interesting prospect for new SERS, and surface-covered substrates in near future.

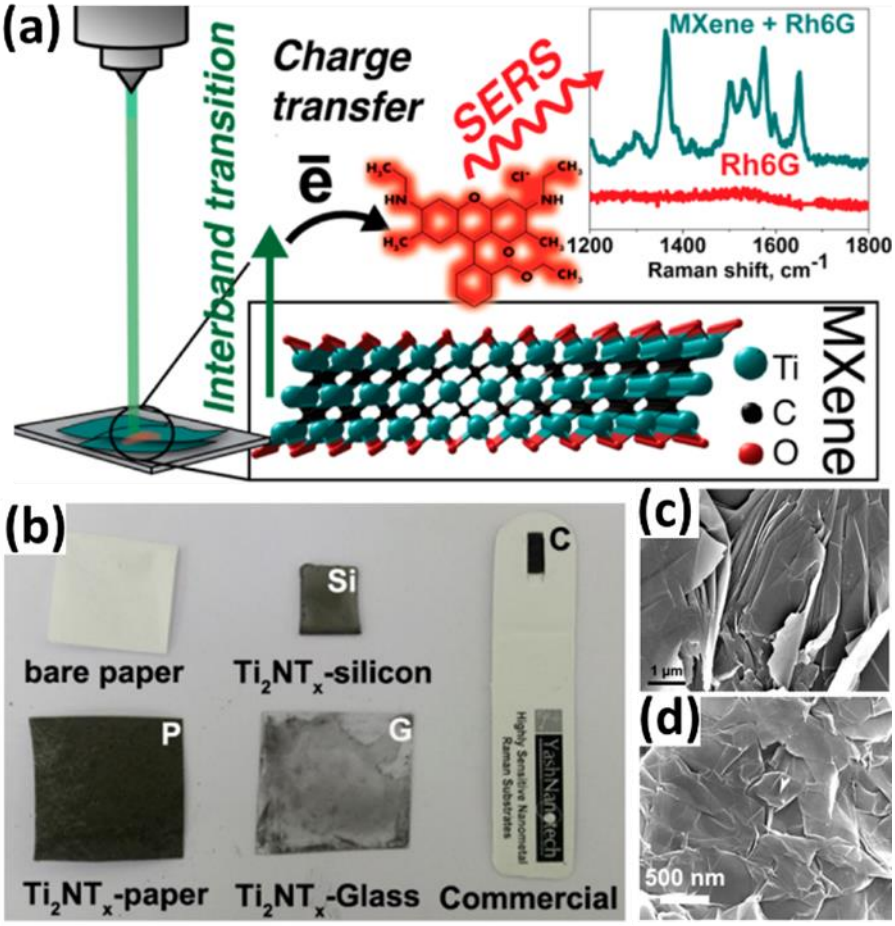

Figure. 15. (a) Schematic illustration of the proposed SERS mechanism. Inter-band transitions in MXene flakes induce strong polarization and charge transfer to the R6G molecule.[229] (b) Photograph of MXenes on different substrates to confirm the flexibility nature. FESEM image of MXenes on (c) glass/silicon-based substrate and (d) paper-based substrates.[230].

6 2D-Transition Metal Chalcogenides for sensing

There are numerous reviews available describing the properties of layered transition metal chalcogenides (2D-TMC)[189,190,206,216,231–235] however reports on the use of 2D-TMC in SERS applications is limited[194,206,216]. These 2D-TMCs facilitate the stable physiochemical interaction between the substrate and organic molecules and interlayer charge transfer [236], and the unique features of thin TMC layers have been investigated as a hybrid structure for SERS enhancement.

6.1 MoX_2 (X = S, Se)

MoS_2, a layered material with unique electronic, optical and mechanical properties has great potential in optoelectronics and energy harvesting application. The honeycomb crystal structure of MoS_2 (**Figure 16a**) is similar to that of graphene and h-BN, but the electronic and surface chemical properties are significantly different. The properties of semiconducting MoS_2 (polar covalent bond) lies between zero-band gap non-polar graphene and wide-band gap (5.9 eV) polar h-BN, providing unique properties for SERS enhancement. In addition to that, the three-layered atomic crystal structure provides surface sites for chemisorption with high oscillator strength in the exciton bands and excitonic resonances, which are also significantly, enhance the SERS signal. A systematic study exploring the characteristics SERS of the same honeycomb-structured graphene, h-BN, and MoS_2 using the CuPc probe molecule, demonstrated different enhancement mechanisms.[23] **Figure 13a** shows the Raman spectra of CuPc molecules on the different substrates. In general, the charge transfer process and interface dipole-dipole interaction with CuPc was responsible for the enhancement factor. In graphene, a non-polar, zero-gap material the strong SERS enhancement was due to charge transfer interaction with CuPc. In contrast, h-BN, a polar insulating material showed strong enhancement due to a dipole-dipole interaction

with CuPc. In MoS_2, both charge transfer and dipole-dipole interactions contributed to the Raman signal enhancement, although the enhancement factor is low compared with h-BN and graphene. Similarly, the comparative studies of MoS_2 and graphene with R6G probe molecule showed a lower enhancement factor for MoS_2 [237]. However, the role of interface charge trap densities between MoS_2 and the probe molecule for enhancement of the Raman signal was demonstrated. Xu *et al.* [238] demonstrated distinct Raman enhancement for an R6G probe molecule at 611, 773, 1361, and 1645 cm^{-1} in the fingerprint region (**Figure 16b-c**). This confirmed both charge transfer and dipole interactions in the enhancement mechanism, and that the enhancement effect was consistent irrespective of MoS_2 layer thickness (number of layer $\leq$3). The preparation of the MoS_2 thin layer in this study, through thermolysis on a mica substrate, might be the reason for the enhanced Raman signal for R6G molecule, because this observation is in contrast to the previous report by Lee *et al.* [237]. In their study, the MoS_2 SERS substrate was mechanically exfoliated from a bulk crystal and mounted on highly *p*-doped silicon substrates. Therefore, the quality of the substrate might be responsible for the difference in enhancement of the SERS signal. Further studies are required to substantiate the results, with the thermal decomposition of MoS_2 on different substrates, and use of other deposition methods, required.

A detailed investigation on the surface properties of MoS_2 nanoflakes, plasma treated MoS_2 and pristine MoS_2 on the enhancement of the Raman spectra of R6G molecules has been conducted [239]. The plasma treated MoS_2 led to the generation of local dipoles and oxygen adsorption on the MoS_2 layer, where the structural disorder induced local dipole and oxygen adsorption provided enhanced Raman scattering. The local dipoles enhance the interaction of R6G due to symmetry variation, whilst oxygen adsorption improves the photo-induced charge

transfer process due to p-doping induced band filling effect (varying electron occupation level in the valence band). In addition, a suspended plasma treated MoS_2 layer and SiO_2 bonded MoS_2 layer showed a similar pattern for R6G indicating a substrate independent enhancement.

A study on various layered structures of MoX_2 (S, Se) displayed the significant Raman enhancement for R6G, CuPc, and CV molecules and revealed interesting possibilities[193]. 1T-MoS_2 exhibits significantly enhanced Raman signals for analytes. 1T-MoX_2 has an octahedral crystal structure with metallic properties and 2H MoX_2 (S, Se) has a trigonal-prismatic coordinated crystal structure with semiconductor properties. **Figure 17a, b** shows the Raman spectra and binding energy plot which, clearly distinguish the 1T- and 2H-MoS_2 phases. The calculated Fermi energies of 1T- and 2H-MoS_2 are -5.013 and -5.866 eV, respectively. For example, the energy level of CuPc LUMO and HOMO are -3.5 and -5.2 eV, respectively, close to the values for 1T-MoS_2. **Figure 17c** shows the Raman spectra of CuPc molecules on different MoX_2 phases and on a blank SiO_2 substrate. The enhancement factors of 2H- and 1T-MoS_2 are 9.2 and 108.6 respectively. This can be explained based on the dominant charge transfer from the metallic 1T-MoS_2 layer. In this case, the dipole interaction is negligible. **Figure 17e-h** depicts the electron transfer process between CuPc and 2H-MoX_2(S/Se) or 1T-MoX_2(S/Se) and demonstrates the significance of associated Fermi energy and electron transition probability for Raman enhancement. The energy transfer process (I and II) is dominant in enhancing the Raman signal in 1T-MoS_2. It is interesting that even though 1T-MoS_2 is metallic, there is no SPR intensity during the detection of 4-nitrothiophenol, which is the prominent probe molecule for metal nanostructures. Similar to 1T-MoS_2, honeycomb 1T-$MoSe_2$ exhibited an enhanced performance (**Figure 17c**)[193], with 1T-$MoSe_2$ showing superior performance for detecting CuPc, R6G, and CV compared to 1T-MoS_2. The enhancement factor of CuPc is 318.4 (108.6 for 1T-

MoS_2). The enhanced enhancement factor was explained based on the Fermi energy (-4.429 eV) of 1T-$MoSe_2$ being less than 1T-MoS_2 (-5.013 eV), hence enabling efficient charge transfer from the higher Fermi energy of 1T-$MoSe_2$ to the HOMO of CuPc, (**Figure 17h**) significantly increasing the electron transition probability and Raman enhancement Also, this 1T-phase material is sensitive to excitation wavelength (**Figure 17d**), which is important because it greatly impacts the charge transfer probability between 1T-MoX_2(S/Se) and the probe molecules.

Apart from the CuPc, R6G, and CV probe molecules, 4-Mercaptopyridine (4-MPy) showed an enhancement factor of 10^5 on a monolayer of MoS_2 [240]. The ultrahigh enhancement for 4-MPy can reasonably be explained based on the fact of laser excitation (488 nm) is in resonance with charge-transfer transitions (467 nm) and exciton resonance (360-390 nm).

Overall, the ability to control the layering of the material (monolayer, bilayer, and multilayer effect) structural disorder, crystal structure transition, surface potential, excitation wavelength, and selection rule of probe molecule provides many opportunities for tuning the functionality of MoX_2 substrates for SERS enhancement.

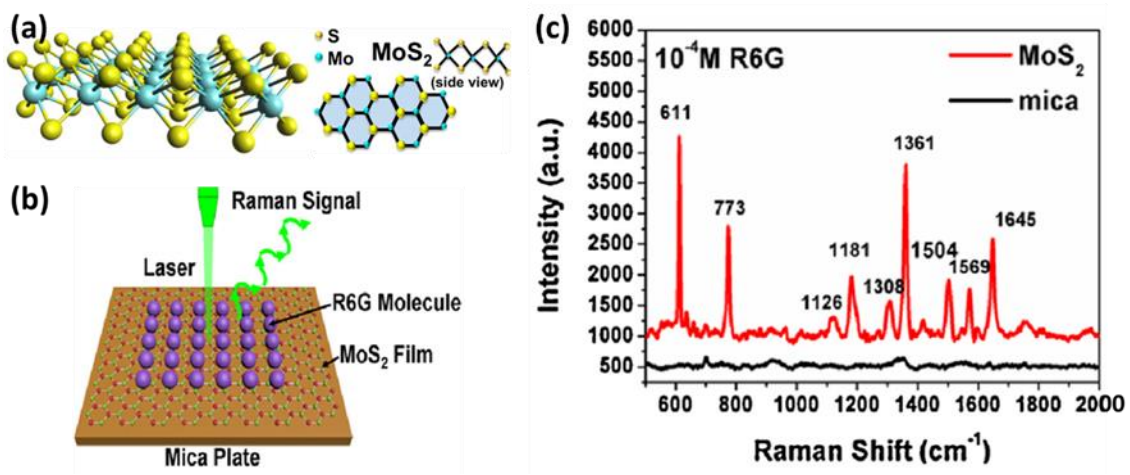

Figure 16. (a) Schematic of layered and honeycomb structure of MoS2 [23,240]; (b, c) Schematic illustration of Raman detection for R6G molecule on monolayer MoS_2 and corresponding Raman spectra of 10^{-4} M R6G from MoS_2 and mica substrates [238]; Excitation wavelength – 532 nm; substrate- mica

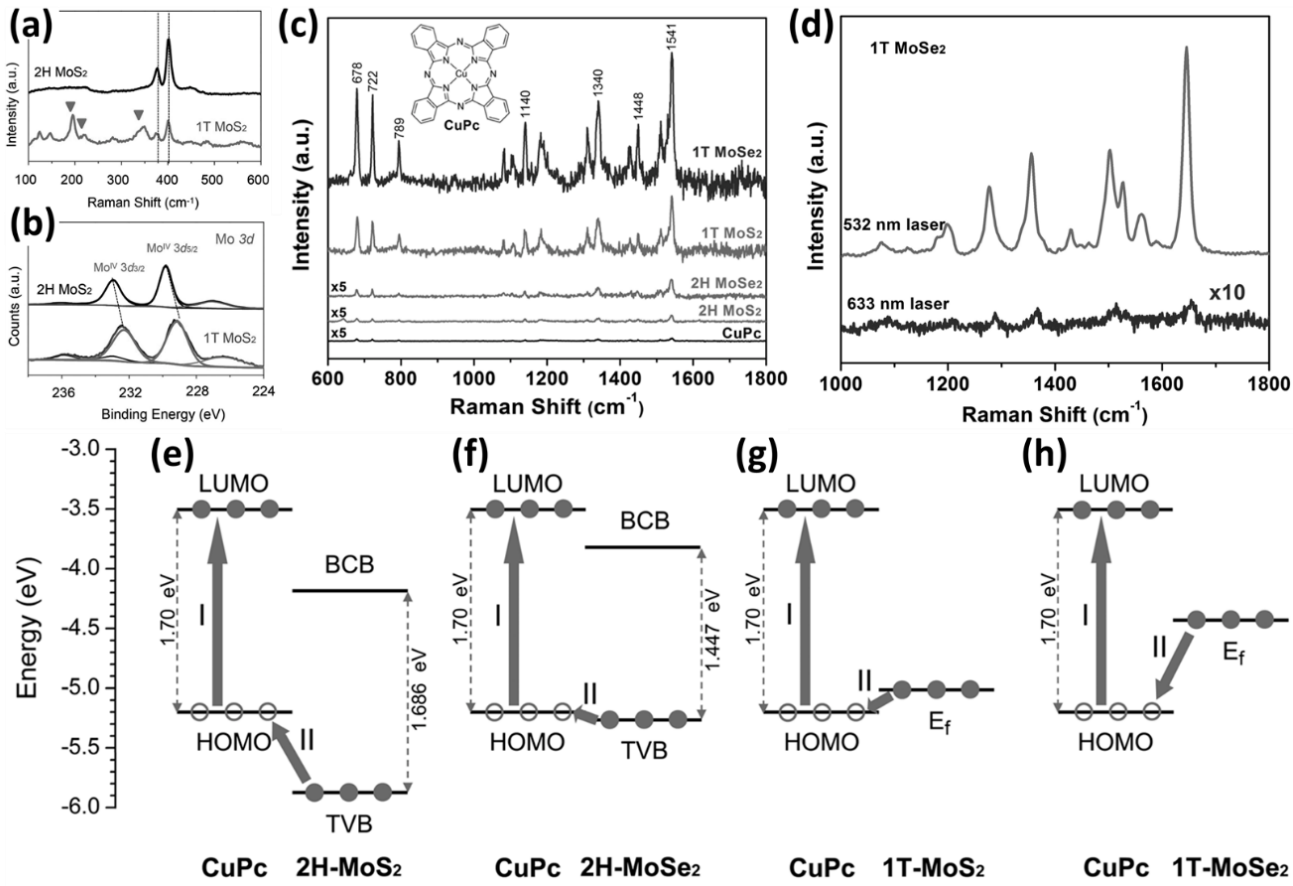

Figure 17. (a, b) Raman spectra and binding energy of 1T- and 2H-MoS_2, (c) Raman spectra of CuPc on 1T-$MoSe_2$, 1T-MoS_2, 2H-$MoSe_2$, 2H-MoS_2 monolayer and SiO_2/Si substrates; Excitation wavelength – 532 nm; CuPc evaporation current – 70 A; time – 5s; (d) Raman spectra of R6G (10^{-5} M) on 1T-$MoSe_2$ substrate excited by 532 and 633 nm laser; substrate - SiO_2/Si (e-h) Schematic illustration of the energy band diagrams and charge transfer process from 2H-MoS2 (e), 2H-$MoSe_2$ (f), 1T-MoS_2 (g), and 1T-$MoSe_2$ (h) monolayers to CuPc. The HOMO and LUMO levels of CuPc, the top of the valence bands (TVB) and the bottom of the conduction bands (BCB) of 2H-MoX_2, and the Fermi energy (E_f) of 1T-MoX_2 are shown in the plot. The black dots and circles represent the electrons and holes, respectively. The symbol I and II represent the different charge transfer process. The band gaps of CuPc and 2H-MoX_2 are represented by dashed lines with arrows [193].

6.2 ReS_2

The anisotropic layered triclinic ReS_2 has highest charge carrier mobility along the zigzag (ZZ) Re atomic chain direction.[235,241] The distorted crystal structure (1T phase) exhibits strong electronic and vibrational decoupling, week intra-layer polarization, and localized charge density along the ZZ chain direction, which facilitates SERS activity (**Figure 18a**).[203,242,243] The anisotropic charge direction in ReS_2 is quite similar to BP (AC direction).[203] The Raman enhancement study of CuPc demonstrated the prominent feature of ReS_2 over BP.[203] The existence of charge distribution along ZZ direction and smaller charge difference between Re and S planes exhibited a strong charge interaction during CuPc adsorption. Miao *et al*.[242] deposited a 5 nm thick aluminum oxide (Al_2O_3) between ReS_2 and R6G to confirm the charge transfer process and **Figure 18b** illustrates the influence of dielectric layer (Al_2O_3) for charge transfer process between substrate and molecule. Furthermore, the monolayer of ReS_2 exhibited an enhanced Raman signal for R6G compared to multi-layer structures [242]. The unique feature of TMC materials is the band gap transition from monolayer to few-layer or bulk, which influences the charge transfer process. The direct band gap (monolayer ReS_2) allows excited electrons in the conduction band to recombine with trapped hole carriers during the charge transfer process. However, direct-to-indirect band transition of the band gap from a monolayer to a few layers might prolong the lifetime of carriers, where recombination reduces the charge transfer process and the Raman scattering. Similarly, excitation energy could influence the charge transfer process and the chemical potential difference between analyte and substrate. Notably, a monolayer of ReS_2 exhibited enhanced resonance Raman scattering with 532 and 633 nm laser excitation for R6G, rhodamine B (RhB), CV and methylene blue (MB), respectively

(**Figure 18c-f**) [242]. The potential of excitation wavelength dependent Raman enhancement for selective chemical sensing opens interesting possibilities for further development.

6.3 WSe_2

The WSe_2 semiconductor layered material, with a honeycomb crystal structure, contains covalently bonded Se-W-Se layers stacked with weak van der Waals force, with an in-plane net dipole moment (for an isolated monolayer) (**Figure 19a**).[244,245] Notably, the crystal structure of WSe_2 is similar to MoS_2, graphene, and h-BN,[23] however its transport properties and in-plane dipole moment give WSe_2 drastically different properties. The SERS of R6G showed strong enhancement factors on mono- and bi-layer WSe_2 at low and high-frequency Raman modes (**Figure 19b**).[237] The evaluation of R6G on WSe_2, in comparison with MoS_2, graphene and bare SiO_2, demonstrated a distinct chemical enhancement for the WSe_2 surface. The analytical enhancement factor of R6G on WSe_2 at low wave number (615 cm^{-1}) was three times higher than observed with MoS_2. Similarly, the observed Raman intensity of WSe_2 exceeded graphene by a factor of 2 at low wave number (<1250 cm^{-1}) and was comparable at higher wave numbers (>1250 cm^{-1}). This suggests that chemical enhancement occurred *via* both charge transfer and dipole interaction phenomenon, and the overall enhancement may therefore be dependent on the in-plane net dipole moment, surface polarity, and energy band structure of WSe_2.

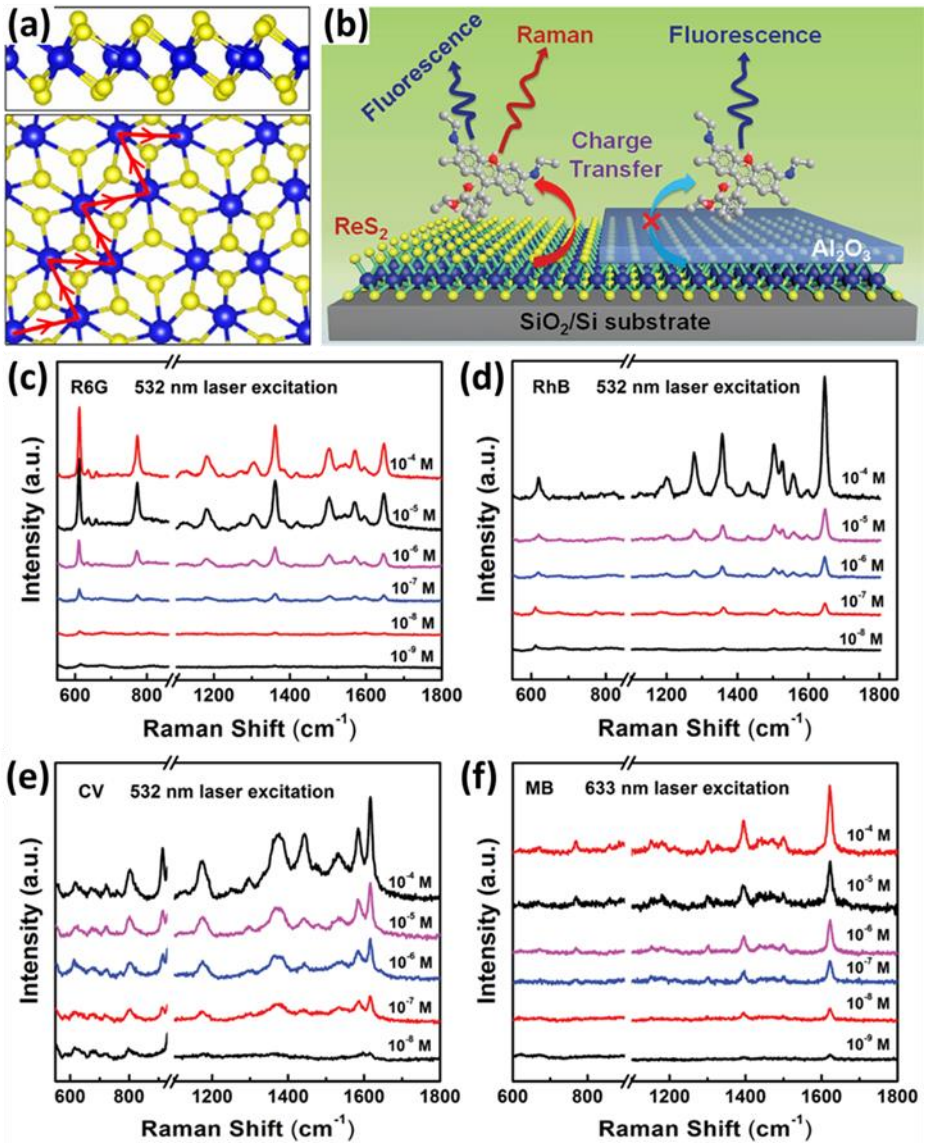

Figure 18. (a). Side and top view of ReS_2 with the distorted 1T crystal structure. The Re atoms dimerize as a result of the Peierls distortion forming a Re chain denoted by the arrowed zigzag line. The blue (dark) and yellow (light) spheres are Re and S atoms, respectively [241]. (b) Schematic illustration of Raman enhancement mechanism on ReS_2 nanosheets. A dielectric layer (Al_2O_3) with a thickness of 5 nm on ReS_2 to block the charge transfer between substrate and analyte molecules [242]. Concentration-dependent Raman spectra of different fluorescent dyes adsorbed on a monolayer of ReS_2 (c) R6G (d) RhB (e) CV and (f) MB.[242] Substrate- SiO_2/Si

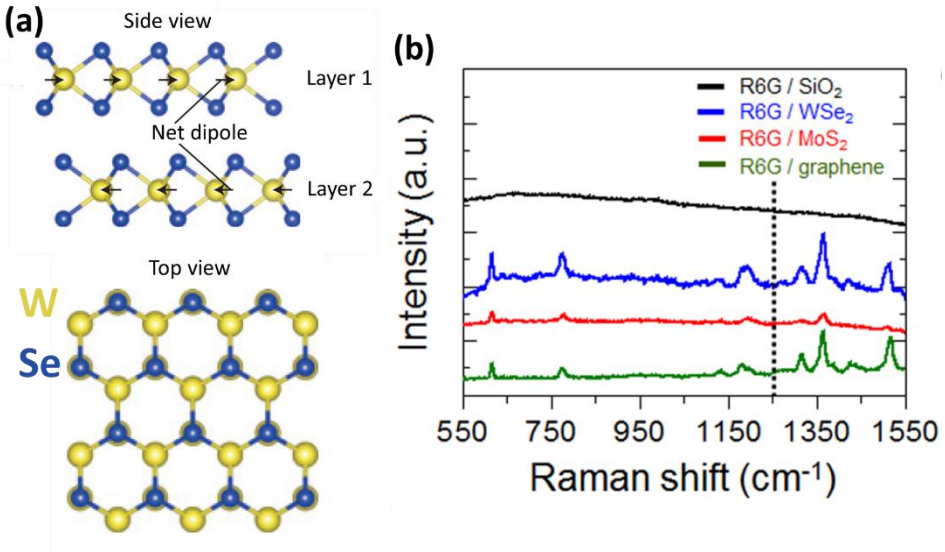

Figure 19. (a) Crystal structure of WSe_2 (side and top views). The unit cell contains two Se-W-Se units in which there is a net in-plane dipole pointing to the right and left, respectively, [244] and (b) Raman spectra of monolayer R6G film adsorbed on the monolayer graphene (green line), MoS_2 (red line), and WSe_2 (blue line) substrates respectively. The dashed black line corresponds to 1250 cm^{-1}. Excitation wavelength – 532 nm; Substrate – p-doped Si on SiO_2; Concentration of R6G - 1μM .[237]

6.4 GaSe

The 2D-layered, *p*-type semiconducting GaSe, has been widely used in nonlinear optical applications.[246,247] The in-plane geometry of GaSe has a honeycomb-like hexagonal structure (four-fold layer with the unique Se-Ga-Ga-Se sequence) (**Figure 20a**). The atomically thin (2D-layer) exhibits unique valance band dispersion which makes it an interesting material for optoelectronic applications.[248] The investigation of SERS effect of GaSe on the CuPc probe molecule demonstrated a fourteen-fold increase in the Raman signal compared to an SiO_2 substrate (**Figure 20b**).[247] The effect of the thickness of GaSe on the enhancement, and demonstration of influence of excitation wavelength for interference enhancement, first layer effect, and resonant Raman scattering, confirms the dominant charge transfer process for the chemical enhancement. Unlike the other 2D materials (MoS_2, and WSe_2), the Raman signal of GaSe follows the charge transfer process alone for chemical enhancement.

6.5 W(Mo)Te_2

The stable 1T' metal tellurides ($MoTe_2$ or WTe_2) exhibit rich electronic properties due to their unusual semi-metallic nature, and in combination with their high surface activities have ideal properties for use as 2D SERS materials. The crystal structure of 1T'-W(Mo)Te_2 (**Figure 20c**)[249] formed with a three-atomic-layer (W-Te-W) stack in [001] axis is more stable compared to other group-VI transition metal dichalcogenides. The high surface activity and low-energy density of states (DOS) of 1T'-WTe_2 was demonstrated to be an ultrasensitive SERS material for detection of trace levels of R6G compared to other reported 2D metal chalcogenides, 2D materials, semiconductors, and noble metals, with Tao *et al.*[212] demonstrating ultrasensitive SERS detection for chemical vapor deposition grown 2D 1T'-W(Mo)Te_2. **Figure 20d** displays the R6G

Raman signatures of different materials, and in comparison with other CVD-derived 2D materials (graphene, WSe_2, 2H-$MoTe_2$, 1T'-$MoTe_2$) 1T'-WTe_2 showed the highest Raman enhancement factor. The semi-metallic property of 1T'-WTe_2 greatly improves the Raman enhancement factor compared to semi-conducting and metallic based SERS materials. The binding energy of 0.67 eV (R6G-WTe_2) and electron transfer is 1.2 e/molecule (WTe_2 to R6G) supports the large charge transfer between the analyte and 1T'-WTe_2, generating a stronger interface dipole. The high surface activity results in the formation of quasi-covalent bonding between R6G-1T'-WTe_2 which strengthens the bond upon dipole electrostatic force to increase the Raman scattering cross-section. Thus, the stronger interface dipole and quasi-covalent bonding in the R6G-1T'-WTe_2 system provides high sensitivity toward the Raman probe.

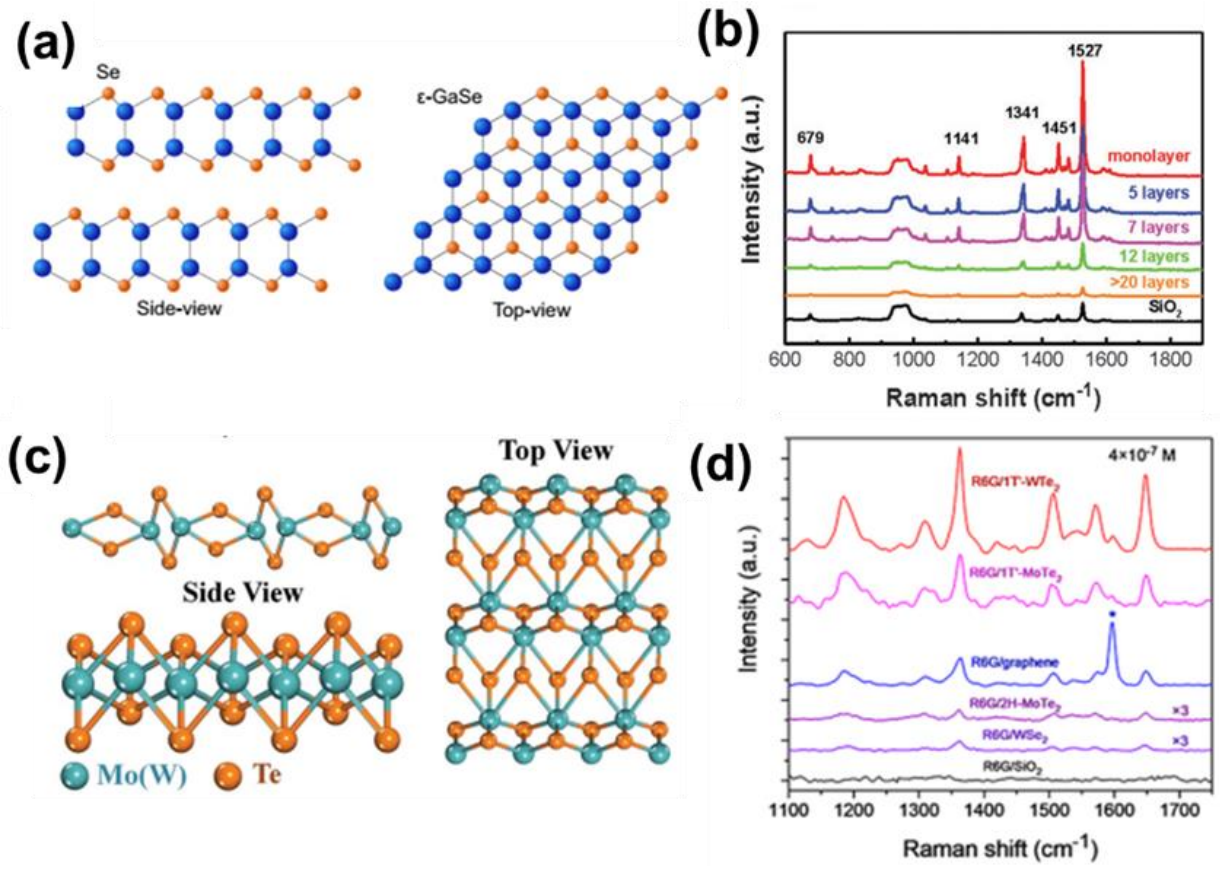

Figure 20. **(a)** Structure of atomically thin GaSe and ε-GaSe [248]. **(b)** Raman spectra of CuPc deposited on the SiO_2/Si substrate and GaSe flakes with different thickness.[247] Excitation wavelength – 514 nm ; thickness of CuPc – 1 nm; **(c)** Side and top views of the crystal structure of 1T'-W(Mo)Te_2[249]. **(d)** Raman spectra of R6G coated on 2d 1T'-WTe_2, 1T'-$MoTe_2$, graphene, 2H-$MoTe_2$, WSe_2, and bare SiO_2 substrates with R6G concentration of 4×10^{-7} M (The Raman peak labelled with "*" is from graphene G mode)[212]. Excitation wavelength – 532 nm ; substrate – SiO_2/Si

7 Challenges and Perspectives

Significant progress has been made on the use of noble metal nanoparticles and their hybrids in SERS-based chemical detection, with parameters such as size, shape, chemical composition and surface characteristics of the metal nanoparticles having a major influence on the SERS-enhancement factor. Metal nanoparticles have a tendency to oxidize in certain chemical environments, and hence nanostructured metal oxide particles have also been used for SERS-enhancement. However pure metal oxide nanoparticles are reported to show very low enhancement factors unless combined with noble metals. Two dimensional inorganic layered materials are promising materials for SERS based chemical sensing because of their layer dependent physical and chemical properties, and enhanced chemical-based charge transfer processes. In the case of graphene, the charge transfer mechanism between the surface and the probe molecule is found to be dependent on several factors, which include number of layers, functionalization, orientation of probe molecules on the surface, first layer effect, equal distribution of analyte molecules, molecular dipole moment and excitation energy of the incident laser. In-depth experimental investigation is very important to analyse the above characteristics and it must be carried out in order to gain a better understanding of the SERS concepts as relevant to 2D materials. The primary challenge for the development of SERS sensors based on 2D layered materials is the reproducible controlled preparation of materials with high purity. As the properties of 2D materials are highly dependent on the number of layers, it is very important to be able to control these properties during materials synthesis. Much of the reported literature on SERS sensors are based on the results obtained from laboratory-scale experiments. However, for real-world application, it is necessary to fabricate 2D materials with wafer compatibility, to

enable direct integration as a miniaturized or portable SERS sensor[250]. For practical applications, the active 2D material must possess some essential properties like robustness, flexibility and stability. In addition to that, several other properties such as high sensitivity, linearity in response, and lack of interference are required for quantification. Currently, it therefore remains challenging to explore 2D materials for designing a smart SERS active substrate, and to further extend the application of 2D materials in SERS sensing it is essential to develop novel stable layered materials with optimized properties such as improved signal reproducibility (less than 20 % variation of the signal intensity) with excellent stability (< 20 % over one month) and non-fluctuating SERS intensity. In addition, novel materials based on nanocomposites of 2D materials with other noble metallic nanostructures should be explored to fabricate active SERS substrates with more efficiency.

8 Conclusion

In this review, recent advances in the use of 2D inorganic nanomaterials towards SERS chemical sensor applications have been presented. The basic theory behind the SERS concept, together with two important mechanisms responsible for SERS enhancement (viz. electromagnetic and chemical), have been described, and a brief overview on the use of various existing nanomaterials as SERS substrates, ranging from traditional metal substrates to advanced hybrid materials, has been highlighted. The chemical enhancement process of various 2D materials, such as graphene and TMC, has been reviewed, and the dominant features responsible for SERS-enhancement in other 2D materials explained, such as the dipole interaction process in h-BN, anisotropic charge flow in black phosphorous, functional group-based synergic enhancement in

MXenes, and the combined effect of both charge transfer and dipole interactions with a probe molecule in TMC. The layer dependent characteristics of 2D TMCs in SERS sensing were also highlighted. There are also several other features such as structural disorders, phase transitions in MoS_2, zigzag charge orientation of an ReS_2 surface, and the in-plane dipole moment of WSe_2 monolayers, that are shown to also have a large influence on the SERS performance. Furthermore, this review article is intended to provide a broad focus on the unique properties of 2D materials, especially the charge transfer interaction between the surface and probe molecules, in order to identify key areas for future research.

Acknowledgements

Dr. PKK would like to acknowledge National Research Foundation of Korea (NRF) for the financial support from the project grant NRF-2016R1D1A1B03934561. This work was supported by the Basic Science Research Program through the National Research Foundation of Korea (NRF) funded by the Ministry of Science, ICT, and Future Planning (NRF-2016R1A2A2A05005327) as well as the Technology Innovation Program funded by the Ministry of Trade, Industry & Energy(MI, Korea) (10047681, Development of Low Cost Conductive Paste Capable of Fine Pattern for Touch Panel and High Conductivity for Solar Cell Using Metal Composite with Core-Shell Structure Prepared by Highly Productive Wet Process).

Biography

Padmanathan Karthick Kannan received his Ph.D. from Madurai Kamaraj University, India under the supervision of Prof. Ramiah Saraswathi. He worked as a PDRA with Dr. C.S. Rout in 2014 at IIT Bhubaneswar, India. In 2016, he joined the research group of Prof. Chan-Hwa Chung at Sungkyunkwan University, South Korea as a Research Professor under Brain-Korea 21 plus fellowship. His present research interest focuses on the development of chemical sensors based on two-dimensional inorganic nanomaterials.

Prabakaran Shankar received his Ph.D. in Nanostructures and Nanotechnologies (2016) from SASTRA University (Thanjavur, India) under the supervision of Prof. John Bosco Balaguru Rayappan. He then moved to Tokai University (Hiratsuka, Japan) as a Postdoctoral Researcher. In 2018, he joined as a Postdoctoral Research Associate in Prof. Jung Heon Lee Research Group at Sungkyunkwan University, South Korea. His current research focuses on the development of 1D-nanomaterials for biomolecule sensing.

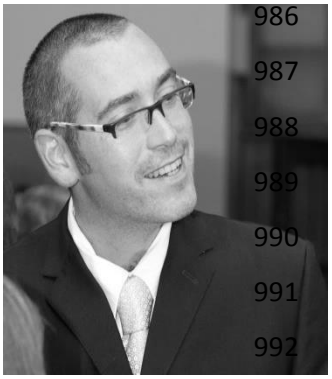

Chris Blackman is a Professor of Inorganic Chemistry in the Department of Chemistry at University College London. His work focuses on the use of vapour deposition techniques (chemical vapour deposition, atomic layer deposition) for synthesis of nanostructured and thin film materials for use in energy and sensing applications. He collaborates with academic groups in the UK and Europe on programmes in materials synthesis, characterization and functional testing, and works with industrial partners to exploit vapour synthesis methods for the manufacture of commercially relevant products.

Chan-Hwa Chung is a Professor of Chemical Engineering at Sungkyunkwan University, South Korea. After holding a Post-doc position (1995-1998) at University of California, Santa-Barbara, he joined Sungkyunkwan University (1999) as a full-time faculty. He also served as the Adjunct Professor at University of New Mexico, NM, USA (2005-2007). He is also the Director of Farad. Materials Co. Ltd, South Korea. His research interests primarily focus on the electrochemical devices and processes such as electrochemical sensors, batteries, supercapacitors, capacitive deionization and electrochemical CO_2 reduction.

References

[1] F.-G. Banica, *Chemical Sensors and Biosensors: Fundamentals and Applications*, John Wiley & Sons, **2012**.

[2] N. A. Zaidi, M. W. Tahir, M. J. Vellekoop, W. Lang, *Sensors* **2017**, *17*.

[3] C. McDonagh, C. S. Burke, B. D. MacCraith, *Chem. Rev.* **2008**, *108*, 400.

[4] B. Fleet, H. Gunasingham, *Talanta* **1992**, *39*, 1449.

[5] D. Li, J. Hu, R. Wu, J. G. Lu, *Nanotechnology* **2010**, *21*, 485502.

[6] S. Fanget, S. Hentz, P. Puget, J. Arcamone, M. Matheron, E. Colinet, P. Andreucci, L. Duraffourg, E. Myers, M. L. Roukes, *Sensors Actuators B Chem.* **2011**, *160*, 804.

[7] A. Lobnik, M. Turel, Š. K. Urek, in *Adv. Chem. Sensors*, InTech, **2012**.

[8] K. Dashtian, R. Zare-Dorabei, *Sensors Actuators B Chem.* **2017**, *242*, 586.

[9] P. A. S. Jorge, P. Caldas, J. C. G. E. da Silva, C. C. Rosa, A. G. Oliva, J. L. Santos, F. Farahi, *Fiber Integr. Opt.* **2005**, *24*, 201.

[10] O. S. Wolfbeis, *J. Mater. Chem.* **2005**, *15*, 2657.

[11] G. Gagliardi, M. Salza, P. Ferraro, E. Chehura, R. P. Tatam, T. K. Gangopadhyay, N. Ballard, D. Paz-Soldan, J. A. Barnes, H.-P. Loock, *Sensors* **2010**, *10*, 1823.

[12] B. Mizaikoff, R. Göbel, R. Krska, K. Taga, R. Kellner, M. Tacke, A. Katzir, *Sensors Actuators B Chem.* **1995**, *29*, 58.

[13] W. Kiefer, *Surface Enhanced Raman Spectroscopy: Analytical, Biophysical and Life Science Applications*, John Wiley & Sons, **2011**.

[14] D. Cialla, S. Pollok, C. Steinbrücker, K. Weber, J. Popp, *Nanophotonics* **2014**, *3*, 383.

[15] E. Garcia-Rico, R. A. Alvarez-Puebla, L. Guerrini, *Chem. Soc. Rev.* **2018**, *47*, 4909.

[16] R. Chen, J. Lin, S. Feng, Z. Huang, G. Chen, J. Wang, Y. Li, H. Zeng, *Appl. Raman Spectrosc. to Biol. Basic Stud. To Dis. Diagnosis* **2012**, 72.

[17] M. Vendrell, K. K. Maiti, K. Dhaliwal, Y.-T. Chang, *Trends Biotechnol.* **2013**, *31*, 249.

[18] T. B. Nguyen, T. K. T. Vu, Q. D. Nguyen, T. D. Nguyen, T. A. Nguyen, T. H. Trinh, *Adv. Nat. Sci. Nanosci. Nanotechnol.* **2012**, *3*, 25016.

[19] A. Lamberti, *Encycl. Nanotechnol.* **2014**, 1.

[20] M. Fan, G. F. S. Andrade, A. G. Brolo, *Anal. Chim. Acta* **2011**, *693*, 7.

[21] W. Xu, N. Mao, J. Zhang, *Small* **2013**, *9*, 1206.

[22] Y. Tan, L. Ma, Z. Gao, M. Chen, F. Chen, *Nano Lett.* **2017**, *17*, 2621.

[23] X. Ling, W. Fang, Y.-H. Lee, P. T. Araujo, X. Zhang, J. F. Rodriguez-Nieva, Y. Lin, J. Zhang, J. Kong, M. S. Dresselhaus, *Nano Lett.* **2014**, *14*, 3033.

[24] C. V. Raman, K. S. Krishnan, *Nature* **1928**, *121*, 501.

[25] A. Kudelski, *Talanta* **2008**, *76*, 1.

[26] F. Yan, M. B. Wabuyele, G. D. Griffin, A. A. Vass, T. Vo-Dinh, *IEEE Sens. J.* **2005**, *5*, 665.

[27] R. Petry, M. Schmitt, J. Popp, *ChemPhysChem* **2003**, *4*, 14.

[28] T. Vankeirsbilck, A. Vercauteren, W. Baeyens, G. Van der Weken, F. Verpoort, G. Vergote, J. P. Remon, *TrAC trends Anal. Chem.* **2002**, *21*, 869.

[29] C. Kallaway, L. M. Almond, H. Barr, J. Wood, J. Hutchings, C. Kendall, N. Stone, *Photodiagnosis Photodyn. Ther.* **2013**, *10*, 207.

[30] C. Krafft, J. Popp, *Anal. Bioanal. Chem.* **2015**, *407*, 699.

[31] N. Stone, P. Matousek, *Cancer Res.* **2008**, *68*, 4424.

[32] Z. Movasaghi, S. Rehman, I. U. Rehman, *Appl. Spectrosc. Rev.* **2007**, *42*, 493.

[33] K. Venkatakrishna, J. Kurien, K. M. Pai, M. Valiathan, N. N. Kumar, C. M. Krishna, G. Ullas, V. B. Kartha, *Curr. Sci.* **2001**, *80*, 665.

[34] H. Tang, C. Zhu, G. Meng, N. Wu, *J. Electrochem. Soc.* **2018**, *165*, B3098.

[35] M. Fleischmann, P. J. Hendra, A. J. McQuillan, *Chem. Phys. Lett.* **1974**, *26*, 163.

[36] D. L. Jeanmaire, R. P. Van Duyne, *J. Electroanal. Chem. Interfacial Electrochem.* **1977**, *84*, 1.

[37] F. Yan, T. Vo-Dinh, *Sensors Actuators B Chem.* **2007**, *121*, 61.

[38] K. E. Shafer-Peltier, C. L. Haynes, M. R. Glucksberg, R. P. Van Duyne, *J. Am. Chem. Soc.* **2003**, *125*, 588.

[39] R. L. Garrell, *Anal. Chem.* **1989**, *61*, 401A.

[40] K. Kneipp, M. Moskovits, H. Kneipp, *Phys. Today* **2007**, *60*, 40.

[41] S. L. McCall, P. M. Platzman, P. A. Wolff, *Phys. Lett. A* **1980**, *77*, 381.

[42] A. Campion, P. Kambhampati, *Chem. Soc. Rev.* **1998**, *27*, 241.

[43] M. Procházka, *Surface-Enhanced Raman Spectroscopy: Bioanalytical, Biomolecular and Medical Applications*, Springer, **2015**.

[44] E. Le Ru, P. Etchegoin, *Principles of Surface-Enhanced Raman Spectroscopy: And Related Plasmonic Effects*, Elsevier, **2008**.

[45] S. P. Mulvaney, C. D. Keating, *Anal. Chem.* **2000**, *72*, 145.

[46] H. A. Szymanski, *Raman Spectroscopy: Theory and Practice*, Springer Science & Business Media, **2012**.

[47] K. Kneipp, H. Kneipp, I. Itzkan, R. R. Dasari, M. S. Feld, *J. Phys. Condens. Matter* **2002**, *14*, R597.

[48] G. McNay, D. Eustace, W. E. Smith, K. Faulds, D. Graham, *Appl. Spectrosc.* **2011**, *65*,

825.

[49] B. Sharma, R. R. Frontiera, A. I. Henry, E. Ringe, R. P. Van Duyne, *Mater. Today* **2012**, *15*, 16.

[50] P. L. Stiles, J. A. Dieringer, N. C. Shah, R. P. Van Duyne, *Annu. Rev. Anal. Chem.* **2008**, *1*, 601.

[51] R. A. Tripp, R. A. Dluhy, Y. Zhao, *Nano Today* **2008**, *3*, 31.

[52] A. Campion, J. E. Ivanecky, C. M. Child, M. Foster, *J. Am. Chem. Soc.* **1995**, *117*, 11807.

[53] M. Moskovits, *J. Raman Spectrosc.* **2005**, *36*, 485.

[54] K. Kneipp, M. Moskovits, H. Kneipp, *Surface-Enhanced Raman Scattering*, **2006**.

[55] S. Schlücker, *Angew. Chemie - Int. Ed.* **2014**, *53*, 4756.

[56] F. Hubenthal, D. B. Sánchez, N. Borg, H. Schmidt, H.-D. Kronfeldt, F. Träger, *Appl. Phys. B* **2009**, *95*, 351.

[57] M. J. Natan, **2003**.

[58] P. Guo, D. Sikdar, X. Huang, K. J. Si, W. Xiong, S. Gong, L. W. Yap, M. Premaratne, W. Cheng, *Nanoscale* **2015**, *7*, 2862.

[59] X. Chen, C. Jiang, S. Yu, *CrystEngComm* **2014**, *16*, 9959.

[60] A. R. Tao, *Pure Appl. Chem.* **2009**, *81*, 61.

[61] A. X. Wang, X. Kong, *Materials (Basel).* **2015**, *8*, 3024.

[62] P. A. Mosier-Boss, *Nanomaterials* **2017**, *7*, 142.

[63] G. Yang, J. Nanda, B. Wang, G. Chen, D. T. Hallinan Jr, *ACS Appl. Mater. Interfaces* **2017**, *9*, 13457.

[64] Y. Yang, S. Matsubara, L. Xiong, T. Hayakawa, M. Nogami, *J. Phys. Chem. C* **2007**, *111*, 9095.

[65] Q. Shao, R. Que, M. Shao, L. Cheng, S. Lee, *Adv. Funct. Mater.* **2012**, *22*, 2067.

[66] M. F. Cardinal, E. Vander Ende, R. A. Hackler, M. O. McAnally, P. C. Stair, G. C. Schatz, R. P. Van Duyne, *Chem. Soc. Rev.* **2017**, *46*, 3886.

[67] F. K. Alsammarraie, M. Lin, *J. Agric. Food Chem.* **2017**, *65*, 666.

[68] S. E. H. Murph, C. J. Murphy, *J. nanoparticle Res.* **2013**, *15*, 1607.

[69] B. Cao, B. Liu, J. Yang, *CrystEngComm* **2013**, *15*, 5735.

[70] Y. Qian, G. Meng, Q. Huang, C. Zhu, Z. Huang, K. Sun, B. Chen, *Nanoscale* **2014**, *6*, 4781.

[71] J. Y. Xu, J. Wang, L. T. Kong, G. C. Zheng, Z. Guo, J. H. Liu, *J. Raman Spectrosc.* **2011**, *42*, 1728.

[72] J.-S. Wi, S. Tominaka, K. Uosaki, T. Nagao, *Phys. Chem. Chem. Phys.* **2012**, *14*, 9131.

[73] G. Das, M. Chirumamilla, A. Gopalakrishnan, A. Toma, S. Panaro, R. P. Zaccaria, F. De Angelis, E. Di Fabrizio, *Microelectron. Eng.* **2013**, *111*, 247.

[74] M. Rycenga, K. K. Hou, C. M. Cobley, A. G. Schwartz, P. H. C. Camargo, Y. Xia, *Phys. Chem. Chem. Phys.* **2009**, *11*, 5903.

[75] Y. Jiang, X.-J. Wu, Q. Li, J. Li, D. Xu, *Nanotechnology* **2011**, *22*, 385601.

[76] Y. Xia, J. Wang, *Mater. Chem. Phys.* **2011**, *125*, 267.

[77] B. Saute, R. Premasiri, L. Ziegler, R. Narayanan, *Analyst* **2012**, *137*, 5082.

[78] A. R. Tao, F. Kim, C. Hess, J. Goldberger, R. He, Y. Sun, Y. Xia, P. Yang, ‖ Andrea Tao †, ‖ Franklin Kim †, ‖ Christian Hess ‡, † Joshua Goldberger, † Rongrui He, § Yugang Sun, § Younan Xia, ‡ and Peidong Yang* †, *Nano Lett.* **2003**, *3*, 1229.

[79] A. Garcia-Leis, J. V. Garcia-Ramos, S. Sanchez-Cortes, *J. Phys. Chem. C* **2013**, *117*, 7791.

[80] T. C. Dao, T. Q. N. Luong, T. A. Cao, N. M. Kieu, V. V. Le, *Adv. Nat. Sci. Nanosci.*

Nanotechnol. **2016**, *7*, DOI 10.1088/2043-6262/7/1/015007.

[81] K. Quester, M. Avalos-Borja, A. R. Vilchis-Nestor, M. A. Camacho-López, E. Castro-Longoria, *PLoS One* **2013**, *8*, e77486.

[82] F. Benz, R. Chikkaraddy, A. Salmon, H. Ohadi, B. de Nijs, J. Mertens, C. Carnegie, R. W. Bowman, J. J. Baumberg, *J. Phys. Chem. Lett.* **2016**, *7*, 2264.

[83] H. W. Cheng, Y. Li, J. Y. Yang, *2010 10th IEEE Conf. Nanotechnology, NANO 2010* **2010**, 732.

[84] F. Tian, F. Bonnier, A. Casey, A. E. Shanahan, H. J. Byrne, *Anal. Methods* **2014**, *6*, 9116.

[85] R. Boyack, E. C. Le Ru, *Phys. Chem. Chem. Phys.* **2009**, *11*, 7398.

[86] J. J. Mock, M. Barbic, D. R. Smith, D. A. Schultz, S. Schultz, *J. Chem. Phys.* **2002**, *116*, 6755.

[87] M. Fan, F.-J. Lai, H.-L. Chou, W.-T. Lu, B.-J. Hwang, A. G. Brolo, *Chem. Sci.* **2013**, *4*, 509.

[88] S. E. Hunyadi, C. J. Murphy, *J. Mater. Chem.* **2006**, *16*, 3929.

[89] K. K. L. Kim, K. K. L. Kim, J. Y. Choi, H. B. Lee, K. S. Shin, *Chem. Phys. Lett.* **2010**, *403*, 3448.

[90] P. Lu, J. Dong, N. Toshima, *Langmuir* **1999**, *15*, 7980.

[91] K. Kim, K. L. Kim, K. S. Shin, *J. Phys. Chem. C* **2011**, *115*, 23374.

[92] G. V. P. Kumar, S. Shruthi, B. Vibha, B. A. A. Reddy, T. K. Kundu, C. Narayana, *J. Phys. Chem. C* **2007**, *111*, 4388.

[93] Y. Yang, J. Shi, G. Kawamura, M. Nogami, *Scr. Mater.* **2008**, *58*, 862.

[94] A. K. Samal, L. Polavarapu, S. Rodal-Cedeira, L. M. Liz-Marzán, J. Pérez-Juste, I. Pastoriza-Santos, *Langmuir* **2013**, *29*, 15076.

[95] L. Cao, P. Diao, L. Tong, T. Zhu, Z. Liu, *ChemPhysChem* **2005**, *6*, 913.

[96] J.-W. Hu, Y. Zhang, J.-F. Li, Z. Liu, B. Ren, S.-G. Sun, Z.-Q. Tian, T. Lian, *Chem. Phys. Lett.* **2005**, *408*, 354.

[97] H. Qian, M. Xu, X. Li, M. Ji, L. Cheng, A. Shoaib, J. Liu, L. Jiang, H. Zhu, J. Zhang, *Nano Res.* **2016**, *9*, 876.

[98] Y. Yin, T. Qiu, L. Ma, X. Lang, Y. Zhang, G. Huang, Y. Mei, O. G. Schmidt, *J. Phys. Chem. C* **2012**, *116*, 25504.

[99] R. A. Alvarez-Puebla, J. P. Bravo-Vasquez, P. Cheben, D.-X. Xu, P. Waldron, H. Fenniri, *J. Colloid Interface Sci.* **2009**, *333*, 237.

[100] L. Wang, F. Wang, L. Shang, C. Zhu, W. Ren, S. Dong, *Talanta* **2010**, *82*, 113.

[101] S.-S. Li, P. Song, A.-J. Wang, J.-J. Feng, *J. Colloid Interface Sci.* **2016**, *482*, 73.

[102] K. Kim, K. L. Kim, K. S. Shin, *J. Phys. Chem. C* **2011**, *115*, 14844.

[103] L. Pei, Y. Ou, W. Yu, Y. Fan, Y. Huang, K. Lai, *J. Nanomater.* **2015**, *16*, 215.

[104] S. Mohan, B. Subramanian, *Procedia Eng.* **2014**, *92*, 19.

[105] J.-F. Li, Y.-J. Zhang, S.-Y. Ding, R. Panneerselvam, Z.-Q. Tian, *Chem. Rev.* **2017**, *117*, 5002.

[106] L. Dai, L. Song, Y. Huang, L. Zhang, X. Lu, J. Zhang, T. Chen, *Langmuir* **2017**, *33*, 5378.

[107] X. Y. Zhu, A. J. Wang, S. S. Chen, X. Luo, J. J. Feng, *Sensors Actuators, B Chem.* **2018**, *260*, 945.

[108] Z. A. Nima, Y. R. Davletshin, F. Watanabe, K. M. Alghazali, J. C. Kumaradas, A. S. Biris, *RSC Adv.* **2017**, *7*, 53164.

[109] H. Portales, L. Saviot, E. Duval, M. Gaudry, E. Cottancin, M. Pellarin, J. Lermé, M. Broyer, *Phys. Rev. B* **2002**, *65*, 165422.

[110] S. Park, P. Yang, P. Corredor, M. J. Weaver, *J. Am. Chem. Soc.* **2002**, *124*, 2428.

[111] M. K. Nguyen, W. N. Su, C. H. Chen, J. Rick, B. J. Hwang, *Spectrochim. Acta - Part A Mol. Biomol. Spectrosc.* **2017**, *175*, 239.

[112] W. Wang, Z. Li, B. Gu, Z. Zhang, H. Xu, *ACS Nano* **2009**, *3*, 3493.

[113] J.-L. Gong, J.-H. Jiang, Y. Liang, G.-L. Shen, R.-Q. Yu, *J. Colloid Interface Sci.* **2006**, *298*, 752.

[114] D. Li, D.-W. Li, Y. Li, J. S. Fossey, Y.-T. Long, *J. Mater. Chem.* **2010**, *20*, 3688.

[115] J. Jin, S. Zhu, Y. Song, H. Zhao, Z. Zhang, Y. Guo, J. Li, W. Song, B. Yang, B. Zhao, *ACS Appl. Mater. Interfaces* **2016**, *8*, 27956.

[116] S. Yi, L. Sun, S. C. Lenaghan, Y. Wang, X. Chong, Z. Zhang, M. Zhang, *RSC Adv.* **2013**, *3*, 10139.

[117] Z. Yi, S. Chen, Y. Chen, J. Luo, W. Wu, Y. Yi, Y. Tang, *Thin Solid Films* **2012**, *520*, 2701.

[118] Z. Yi, X. Tan, G. Niu, X. Xu, X. Li, X. Ye, J. Luo, B. Luo, W. Wu, Y. Tang, *Appl. Surf. Sci.* **2012**, *258*, 5429.

[119] S.-S. Chen, X.-X. Lin, A.-J. Wang, H. Huang, J.-J. Feng, *Sensors Actuators B Chem.* **2017**, *248*, 214.

[120] Y.-H. Lai, S.-C. Kuo, Y.-C. Hsieh, Y.-C. Tai, W.-H. Hung, U.-S. Jeng, *RSC Adv.* **2016**, *6*, 13185.

[121] J. Ji, P. Li, S. Sang, W. Zhang, Z. Zhou, X. Yang, H. Dong, G. Li, J. Hu, *AIP Adv.* **2014**, *4*, 31329.

[122] G. Hunter, J. Xu, L. Evans, R. Vander Wal, G. Berger, C. C. Liu, *ECS Trans.* **2006**, *3*, 199.

[123] A. Pérez-Tomás, A. Mingorance, D. Tanenbaum, M. Lira-Cantú, in *Futur. Semicond. Oxides Next-Generation Sol. Cells*, Elsevier, **2018**, pp. 267–356.

[124] X. Yu, T. J. Marks, A. Facchetti, *Nat. Mater.* **2016**, *15*, 383.

[125] Y. Zhang, L. Li, H. Su, W. Huang, X. Dong, *J. Mater. Chem. A* **2015**, *3*, 43.

[126] X. Guo, G. Zhang, Q. Li, H. Xue, H. Pang, *Energy Storage Mater.* **2018**, *15*, 171.

[127] J. Desilvestro, O. Haas, *J. Electrochem. Soc.* **1990**, *137*, 5C.

[128] M. C. Toroker, E. A. Carter, *J. Mater. Chem. A* **2013**, *1*, 2474.

[129] G. F. Fine, L. M. Cavanagh, A. Afonja, R. Binions, *Sensors* **2010**, *10*, 5469.

[130] A. A. Tomchenko, G. P. Harmer, B. T. Marquis, J. W. Allen, *Sensors Actuators B Chem.* **2003**, *93*, 126.

[131] K. Wetchakun, T. Samerjai, N. Tamaekong, C. Liewhiran, C. Siriwong, V. Kruefu, A. Wisitsoraat, A. Tuantranont, S. Phanichphant, *Sensors Actuators B Chem.* **2011**, *160*, 580.

[132] H. Yamada, Y. Yamamoto, N. Tani, *Chem. Phys. Lett.* **1982**, *86*, 397.

[133] H. Yamada, Y. Yamamoto, *Surf. Sci.* **1983**, *134*, 71.

[134] Q. Zhou, G. Meng, Q. Huang, C. Zhu, H. Tang, Y. Qian, B. Chen, B. Chen, *Phys. Chem. Chem. Phys.* **2014**, *16*, 3686.

[135] J. Prakash, S. Sun, H. C. Swart, R. K. Gupta, *Appl. Mater. Today* **2018**, *11*, 82.

[136] W. Song, Y. Wang, B. Zhao, *J. Phys. Chem. C* **2007**, *111*, 12786.

[137] M. A. Khan, T. P. Hogan, B. Shanker, *J. Raman Spectrosc.* **2009**, *40*, 1539.

[138] Y. B. Li, Y. Bando, T. Sato, K. Kurashima, *Appl. Phys. Lett.* **2002**, *81*, 144.

[139] X. D. Bai, P. X. Gao, Z. L. Wang, E. G. Wang, *Appl. Phys. Lett.* **2003**, *82*, 4806.

[140] Y. B. Li, Y. Bando, D. Golberg, *Appl. Phys. Lett.* **2004**, *84*, 3603.

[141] L. Vayssieres, *Adv. Mater.* **2003**, *15*, 464.

[142] L. Liu, K. Hong, X. Ge, D. Liu, M. Xu, *J. Phys. Chem. C* **2014**, *118*, 15551.

[143] Y. Zhang, J. Chung, J. Lee, J. Myoung, S. Lim, *J. Phys. Chem. Solids* **2011**, *72*, 1548.

[144] L. Yang, Y. Yang, Y. Ma, S. Li, Y. Wei, Z. Huang, N. V. Long, *Nanomaterials* **2017**, *7*, 398.

[145] G. Shan, S. Zheng, S. Chen, Y. Chen, Y. Liu, *Colloids Surfaces B Biointerfaces* **2012**, *94*, 157.

[146] L. Sun, D. Zhao, M. Ding, H. Zhao, Z. Zhang, B. Li, D. Shen, *Appl. Surf. Sci.* **2012**, *258*, 7813.

[147] W. Song, Y. Wang, H. Hu, B. Zhao, *J. Raman Spectrosc.* **2007**, *38*, 1320.

[148] L. Chen, L. Luo, Z. Chen, M. Zhang, J. A. Zapien, C. S. Lee, S. T. Lee, *J. Phys. Chem. C* **2009**, *114*, 93.

[149] X. W. Lou, D. Deng, J. Y. Lee, J. Feng, L. A. Archer, *Adv. Mater.* **2008**, *20*, 258.

[150] M. Gao, G. Xing, J. Yang, L. Yang, Y. Zhang, H. Liu, H. Fan, Y. Sui, B. Feng, Y. Sun, *Microchim. Acta* **2012**, *179*, 315.

[151] Q. Tao, S. Li, C. Ma, K. Liu, Q.-Y. Zhang, *Dalt. Trans.* **2015**, *44*, 3447.

[152] M. R. Mahoney, R. P. Cooney, *J. Chem. Soc. Faraday Trans. 1 Phys. Chem. Condens. Phases* **1985**, *81*, 2123.

[153] G. Xue, Q. Shen, J. Dong, *J. Chem. Soc. Faraday Trans.* **1991**, *87*, 1021.

[154] Q. Dai, M. Ma, *Spectrosc. Lett.* **1995**, *28*, 43.

[155] A. Kudelski, W. Grochala, M. Janik-Czachor, J. Bukowska, A. Szummer, M. Dolata, *J. Raman Spectrosc.* **1998**, *29*, 431.

[156] Y. WANG, H. HU, S. JING, Y. WANG, Z. SUN, B. ZHAO, C. ZHAO, J. R. LOMBARDI, *Anal. Sci.* **2007**, *23*, 787.

[157] P. Sheng, W. Li, P. Du, K. Cao, Q. Cai, *Talanta* **2016**, *160*, 537.

[158] S.-Y. Fu, Y.-K. Hsu, M.-H. Chen, C.-J. Chuang, Y.-C. Chen, Y.-G. Lin, *Opt. Express* **2014**, *22*, 14617.

[159] K. Xu, H. Yan, C. F. Tan, Y. Lu, Y. Li, G. W. Ho, R. Ji, M. Hong, *Adv. Opt. Mater.* **2018**, *6*, 1701167.

[160] S. Kumar, D. K. Lodhi, J. P. Singh, *RSC Adv.* **2016**, *6*, 45120.

[161] Y.-C. Lai, H.-C. Ho, B.-W. Shih, F.-Y. Tsai, C.-H. Hsueh, *Appl. Surf. Sci.* **2018**, *439*, 852.

[162] L.-L. Qu, N. Wang, G. Zhu, T. P. Yadav, X. Shuai, D. Bao, G. Yang, D. Li, H. Li, *Talanta* **2018**, *186*, 265.

[163] L. J. Oblonsky, S. Virtanen, V. Schroeder, T. M. Devine, *J. Electrochem. Soc.* **1997**, *144*, 1604.

[164] C. R. Wang, Z. F. Zhou, Y. J. Li, R. R. Tian, X. C. Dai, in *New Mater. Adv. Mater.*, Trans Tech Publications, **2011**, pp. 67–72.

[165] L. Zhang, Z. Bao, X. Yu, P. Dai, J. Zhu, M. Wu, G. Li, X. Liu, Z. Sun, C. Chen, *ACS Appl. Mater. Interfaces* **2016**, *8*, 6431.

[166] X. Fu, F. Bei, X. Wang, X. Yang, L. Lu, *J. Raman Spectrosc.* **2009**, *40*, 1290.

[167] X. Zhang, Y. Niu, J. Zhao, Y. Li, *Colloids Surfaces A Physicochem. Eng. Asp.* **2017**, *520*, 343.

[168] D. A. Wheeler, S. A. Adams, T. López-Luke, A. Torres-Castro, J. Z. Zhang, *Ann. Phys.* **2012**, *524*, 670.

[169] A. Mezni, I. Balti, A. Mlayah, N. Jouini, L. S. Smiri, *J. Phys. Chem. C* **2013**, *117*, 16166.

[170] X. Tang, R. Dong, L. Yang, J. Liu, *J. Raman Spectrosc.* **2015**, *46*, 470.

[171] Z. Wang, L. Wu, F. Wang, Z. Jiang, B. Shen, *J. Mater. Chem. A* **2013**, *1*, 9746.

[172] Z. Sun, J. Du, F. Duan, K. He, C. Jing, *J. Mater. Chem. C* **2018**, *6*, 2252.

[173] H. Lai, F. Xu, L. Wang, *J. Mater. Sci.* **2018**, *53*, 8677.

[174] K. Xu, H. Yan, C. F. Tan, Y. Lu, Y. Li, G. W. Ho, R. Ji, M. Hong, *Adv. Opt. Mater.* **2018**, *6*, 1.

[175] L. Ma, Y. Huang, M. Hou, Z. Xie, Z. Zhang, *Sci. Rep.* **2015**, *5*, 1.

[176] L. Bachenheimer, P. Elliott, S. Stagon, H. Huang, *Appl. Phys. Lett.* **2014**, *105*, 1.

[177] S. Hsieh, P. Y. Lin, L. Y. Chu, *J. Phys. Chem. C* **2014**, *118*, 12500.

[178] D. Han, H. Huang, D. Du, X. Lang, K. Long, Q. Hao, T. Qiu, *Mater. Chem. Phys.* **2015**, *153*, 88.

[179] J. Wang, F. Cui, S. Chu, X. Jin, J. Pu, Z. Wang, *Chempluschem* **2014**, *79*, 684.

[180] A. K. Pal, S. Pagal, K. Prashanth, G. K. Chandra, S. Umapathy, B. M. D., *Sensors Actuators, B Chem.* **2019**, *279*, 157.

[181] Y. Liu, *Mater. Lett.* **2018**, *224*, 26.

[182] W. Ren, Z. Zhou, J. M. K. Irudayaraj, *Analyst* **2015**, *140*, 6625.

[183] S. C. Xu, Y. X. Zhang, Y. Y. Luo, S. Wang, H. L. Ding, J. M. Xu, G. H. Li, *Analyst* **2013**, *138*, 4519.

[184] Y. Zhao, L. Sun, M. Xi, Q. Feng, C. Jiang, H. Fong, *ACS Appl. Mater. Interfaces* **2014**, *6*, 5759.

[185] X. He, H. Wang, Q. Zhang, Z. Li, X. Wang, *Eur. J. Inorg. Chem.* **2014**, *2014*, 2432.

[186] Y. Xie, T. Chen, Y. Guo, Y. Cheng, H. Qian, W. Yao, *Food Chem.* **2019**, *270*, 173.

[187] V. Ranc, Z. Markova, M. Hajduch, R. Prucek, L. Kvitek, J. Kaslik, K. Safarova, R. Zboril, *Anal. Chem.* **2014**, *86*, 2939.

[188] S. Yang, D. Slotcavage, J. D. Mai, F. Guo, S. Li, Y. Zhao, Y. Lei, C. E. Cameron, T. J. Huang, *J. Mater. Chem. C* **2014**, *2*, 8350.

[189] S. Zhang, N. Zhang, Y. Zhao, T. Cheng, X. Li, R. Feng, H. Xu, Z. Liu, J. Zhang, L. Tong, *Chem. Soc. Rev.* **2018**, *47*, 3217.

[190] X. Lu, X. Luo, J. Zhang, S. Y. Quek, Q. Xiong, *Lattice Vibrations and Raman Scattering in Two-Dimensional Layered Materials beyond Graphene*, **2016**.

[191] L. Sun, H. Hu, D. Zhan, J. Yan, L. Liu, J. S. Teguh, E. K. L. Yeow, P. S. Lee, Z. Shen, *Small* **2014**, *10*, 1090.

[192] Z. Zheng, S. Cong, W. Gong, J. Xuan, G. Li, W. Lu, F. Geng, Z. Zhao, *Nat. Commun.* **2017**, *8*, 2.

[193] Y. Yin, P. Miao, Y. Zhang, J. Han, X. Zhang, Y. Gong, L. Gu, C. Xu, T. Yao, P. Xu, Y. Wang, B. Song, S. Jin, *Adv. Funct. Mater.* **2017**, *27*, 1606694.

[194] N. Zhang, L. Tong, J. Zhang, *Chem. Mater.* **2016**, *28*, 6426.

[195] X. Ling, L. Xie, Y. Fang, H. Xu, H. Zhang, J. Kong, M. S. Dresselhaus, J. Zhang, Z. Liu, *Nano Lett.* **2010**, *10*, 553.

[196] X. Ling, J. Zhang, *Small* **2010**, *6*, 2020.

[197] A. Otto, *Phys. status solidi* **2001**, *188*, 1455.

[198] S. Huang, X. Ling, L. Liang, Y. Song, W. Fang, J. Zhang, J. Kong, V. Meunier, M. S. Dresselhaus, *Nano Lett.* **2015**, *15*, 2892.

[199] X. Ling, J. Wu, W. Xu, J. Zhang, *Small* **2012**, *8*, 1365.

[200] J. Cabalo, J. A. Guicheteau, S. Christesen, *J. Phys. Chem. A* **2013**, *117*, 9028.

[201] Y. Joo, M. Kim, C. Kanimozhi, P. Huang, B. M. Wong, S. Singha Roy, M. S. Arnold, P. Gopalan, *J. Phys. Chem. C* **2016**, *120*, 13815.

[202] X. Ling, J. Wu, L. Xie, J. Zhang, *J. Phys. Chem. C* **2013**, *117*, 2369.

[203] J. Lin, L. Liang, X. Ling, S. Zhang, N. Mao, N. Zhang, B. G. Sumpter, V. Meunier, L. Tong, J. Zhang, *J. Am. Chem. Soc.* **2015**, *137*, 15511.

[204] J. Wu, S. Zhang, D. Lin, B. Ma, L. Yang, S. Zhang, L. Kang, N. Mao, N. Zhang, L. Tong, J. Zhang, *Adv. Mater. Interfaces* **2018**, *5*, 1700941.

[205] W. Xu, N. Mao, J. Zhang, *Small* **2013**, *9*, 1206.

[206] M. Xia, *Coatings* **2018**, *8*, 137.

[207] X. Ling, L. G. Moura, M. A. Pimenta, J. Zhang, *J. Phys. Chem. C* **2012**, *116*, 25112.

[208] C. Y. Chen, D. P. Wong, Y. F. Huang, H. T. Lien, P. C. Chiang, P. L. Li, F. Y. Shih, W. H. Wang, K. H. Chen, L. C. Chen, Y. F. Chen, *ACS Photonics* **2016**, *3*, 985.

[209] S. Sun, Z. Zhang, P. Wu, *ACS Appl. Mater. Interfaces* **2013**, *5*, 5085.

[210] Z. Fan, R. Kanchanapally, P. C. Ray, *J. Phys. Chem. Lett.* **2013**, *4*, 3813.

[211] D. Liu, X. Chen, Y. Hu, T. Sun, Z. Song, Y. Zheng, Y. Cao, Z. Cai, M. Cao, L. Peng, Y. Huang, L. Du, W. Yang, G. Chen, D. Wei, A. T. S. Wee, D. Wei, *Nat. Commun.* **2018**, *9*, 193.

[212] L. Tao, K. Chen, Z. Chen, C. Cong, C. Qiu, J. Chen, X. Wang, H. Chen, T. Yu, W. Xie, S. Deng, J.-B. Bin Xu, *J. Am. Chem. Soc.* **2018**, *140*, 8696.

[213] C. R. Dean, A. F. Young, I. Meric, C. Lee, L. Wang, S. Sorgenfrei, K. Watanabe, T. Taniguchi, P. Kim, K. L. Shepard, J. Hone, *Nat. Nanotechnol.* **2010**, *5*, 722.

[214] L. H. Li, Y. Chen, *Adv. Funct. Mater.* **2016**, *26*, 2594.

[215] K. Zhang, Y. Feng, F. Wang, Z. Yang, J. Wang, *J. Mater. Chem. C* **2017**, *5*, 11992.

[216] M. Xia, *Int. J. Spectrosc.* **2018**, *2018*, 1.

[217] Q. Cai, D. Scullion, A. Falin, K. Watanabe, T. Taniguchi, Y. Chen, E. J. G. Santos, L. H. Li, *Nanoscale* **2017**, *9*, 3059.

[218] Q. Cai, L. H. Li, Y. Yu, Y. Liu, S. Huang, Y. Chen, K. Watanabe, T. Taniguchi, *Phys. Chem. Chem. Phys.* **2015**, *17*, 7761.

[219] Q. Cai, S. Mateti, W. Yang, R. Jones, K. Watanabe, T. Taniguchi, S. Huang, Y. Chen, L. H. Li, *Angew. Chemie - Int. Ed.* **2016**, *55*, 8405.

[220] J. Wang, F. Ma, W. Liang, R. Wang, M. Sun, *Nanophotonics* **2017**, *6*, 943.

[221] G. Kim, M. Kim, C. Hyun, S. Hong, K. Y. Ma, H. S. Shin, H. Lim, *ACS Nano* **2016**, *10*, 11156.

[222] F. Xia, H. Wang, Y. Jia, *Nat. Commun.* **2014**, *5*, 1.

[223] L. Li, Y. Yu, G. J. Ye, Q. Ge, X. Ou, H. Wu, D. Feng, X. H. Chen, Y. Zhang, *Nat. Nanotechnol.* **2014**, *9*, 372.

[224] J. Wu, N. Mao, L. Xie, H. Xu, J. Zhang, *Angew. Chemie Int. Ed.* **2015**, *54*, 2366.

[225] H. B. Ribeiro, M. A. Pimenta, C. J. S. de Matos, *J. Raman Spectrosc.* **2017**, 76.

[226] H. Liu, A. T. Neal, Z. Zhu, Z. Luo, X. Xu, D. Tománek, P. D. Ye, *ACS Nano* **2014**, *8*, 4033.

[227] M. Naguib, M. Kurtoglu, V. Presser, J. Lu, J. Niu, M. Heon, L. Hultman, Y. Gogotsi, M. W. Barsoum, *Adv. Mater.* **2011**, *23*, 4248.

[228] K. Huang, Z. Li, J. Lin, G. Han, P. Huang, *Chem. Soc. Rev.* **2018**, DOI 10.1039/C7CS00838D.

[229] A. Sarycheva, T. Makaryan, K. Maleski, E. Satheeshkumar, A. Melikyan, H. Minassian, M. Yoshimura, Y. Gogotsi, *J. Phys. Chem. C* **2017**, *121*, 19983.

[230] B. Soundiraraju, B. K. George, *ACS Nano* **2017**, *11*, 8892.

[231] X. Zhang, X.-F. Qiao, W. Shi, J.-B. Wu, D.-S. Jiang, P.-H. Tan, *Chem. Soc. Rev.* **2015**, *44*, 2757.

[232] M. Samadi, N. Sarikhani, M. Zirak, H. Zhang, H. Zhang, A. Z. Moshfegh, *Nanoscale Horizons* **2017**, *3*, 90.

[233] S. Z. Butler, S. M. Hollen, L. Cao, Y. Cui, J. A. Gupta, H. R. Gutiérrez, T. F. Heinz, S. S.

Hong, J. Huang, A. F. Ismach, E. Johnston-Halperin, M. Kuno, V. V. Plashnitsa, R. D. Robinson, R. S. Ruoff, S. Salahuddin, J. Shan, L. Shi, M. G. Spencer, M. Terrones, W. Windl, J. E. Goldberger, *ACS Nano* **2013**, *7*, 2898.

[234] Q. H. Wang, K. Kalantar-Zadeh, A. Kis, J. N. Coleman, M. S. Strano, *Nat. Nanotechnol.* **2012**, *7*, 699.

[235] M. Rahman, K. Davey, S. Z. Qiao, *Adv. Funct. Mater.* **2017**, *27*, DOI 10.1002/adfm.201606129.

[236] T. Shimada, K. Hamaguchi, A. Koma, F. S. Ohuchi, *Appl. Phys. Lett.* **1998**, *72*, 1869.

[237] Y. Lee, H. Kim, J. Lee, S. H. Yu, E. Hwang, C. Lee, J. H. Ahn, J. H. Cho, *Chem. Mater.* **2016**, *28*, 180.

[238] Y. Y. Xu, C. Yang, S. Z. Jiang, B. Y. Man, M. Liu, C. S. Chen, C. Zhang, Z. C. Sun, H. W. Qiu, H. S. Li, D. J. Feng, J. X. Zhang, *Appl. Surf. Sci.* **2015**, *357*, 1708.

[239] L. Sun, H. Hu, D. Zhan, J. Yan, L. Liu, J. S. Teguh, E. K. L. Yeow, P. S. Lee, Z. Shen, *Small* **2014**, *10*, 1090.

[240] C. Muehlethaler, C. R. Considine, V. Menon, W. C. Lin, Y. H. Lee, J. R. Lombardi, *ACS Photonics* **2016**, *3*, 1164.

[241] S. Tongay, H. Sahin, C. Ko, A. Luce, W. Fan, K. Liu, J. Zhou, Y.-S. Huang, C.-H. Ho, J. Yan, *Nat. Commun.* **2014**, *5*, 3252.

[242] P. Miao, J.-K. Qin, Y. Shen, H. Su, J. Dai, B. Song, Y. Du, M. Sun, W. Zhang, H.-L. Wang, C.-Y. Xu, P. Xu, *Small* **2018**, *14*, 1704079.

[243] D. Wolverson, S. Crampin, A. S. Kazemi, A. Ilie, S. J. Bending, *ACS Nano* **2014**, *8*, 11154.

[244] J. M. Riley, F. Mazzola, M. Dendzik, M. Michiardi, T. Takayama, L. Bawden, C. Granerød, M. Leandersson, T. Balasubramanian, M. Hoesch, T. K. Kim, H. Takagi, W. Meevasana, P. Hofmann, M. S. Bahramy, J. W. Wells, P. D. C. King, *Nat. Phys.* **2014**, *10*,

835.

[245] R. Addou, R. M. Wallace, *ACS Appl. Mater. Interfaces* **2016**, *8*, 26400.

[246] N. C. Fernelius, *Prog. Cryst. Growth Charact. Mater.* **1994**, *28*, 275.

[247] L. Quan, Y. Song, Y. Lin, G. Zhang, Y. Dai, Y. Wu, K. Jin, H. Ding, N. Pan, Y. Luo, X. Wang, *J. Mater. Chem. C* **2015**, *3*, 11129.

[248] M.-W. Chen, H. Kim, D. Ovchinnikov, A. Kuc, T. Heine, O. Renault, A. Kis, *npj 2D Mater. Appl.* **2018**, *2*, 2.

[249] K. Chen, Z. Chen, X. Wan, Z. Zheng, F. Xie, W. Chen, X. Gui, H. Chen, W. Xie, J. Xu, *Adv. Mater.* **2017**, *29*, 1700704.

[250] R. Shi, X. Liu, Y. Ying, *J. Agric. Food Chem.* **2018**, *66*, 6525.